



US 20250259375A1

(19) United States

(12) Patent Application Publication (10) Pub. No.: US 2025/0259375 A1

Gu et al.

(43) Pub. Date: Aug. 14, 2025

(54) EFFICIENT RAY-TRACING RENDERING PROCESSOR WITH OPTIMIZATION FOR MOBILE DEVICES AND SUPPORT OF INVERSE RENDERING

(71) Applicant: Northwestern University, Evanston, IL (US)

(72) Inventors: Jie Gu, Evanston, IL (US); Shiyu Guo, Chicago, IL (US)

(21) Appl. No.: 19/053,742

(22) Filed: Feb. 14, 2025

Related U.S. Application Data

(60) Provisional application No. 63/553,331, filed on Feb. 14, 2024.

Publication Classification

(51) Int. Cl.

G06T 15/06 (2011.01)

G06T 15/00 (2011.01)

(52) U.S. Cl.

CPC G06T 15/06 (2013.01); G06T 15/005 (2013.01)

ABSTRACT

In certain aspects, application-specific integrated circuit (ASIC) comprises a global ray-tracing scheduler (GRTS) in communication with a processing element (PE) array. The ASIC comprises a global memory access controller (GMAC) in communication with the PE array and the GRTS. The ASIC comprises a physical attributes MEM (PAMEM) in communication with the GRTS. The ASIC comprises a reconfigurable mixed-precision processing element of the PE array configured to support an inverse rendering mode for background extraction and a ray-tracing mode.

50

52

Ray-Tracing Rendering Algorithm

54

56

58

① Ray Generation

$$r(t) = o + td$$

② Intersect Computation

1. Bounding Box Intersection
2. Triangle Intersection

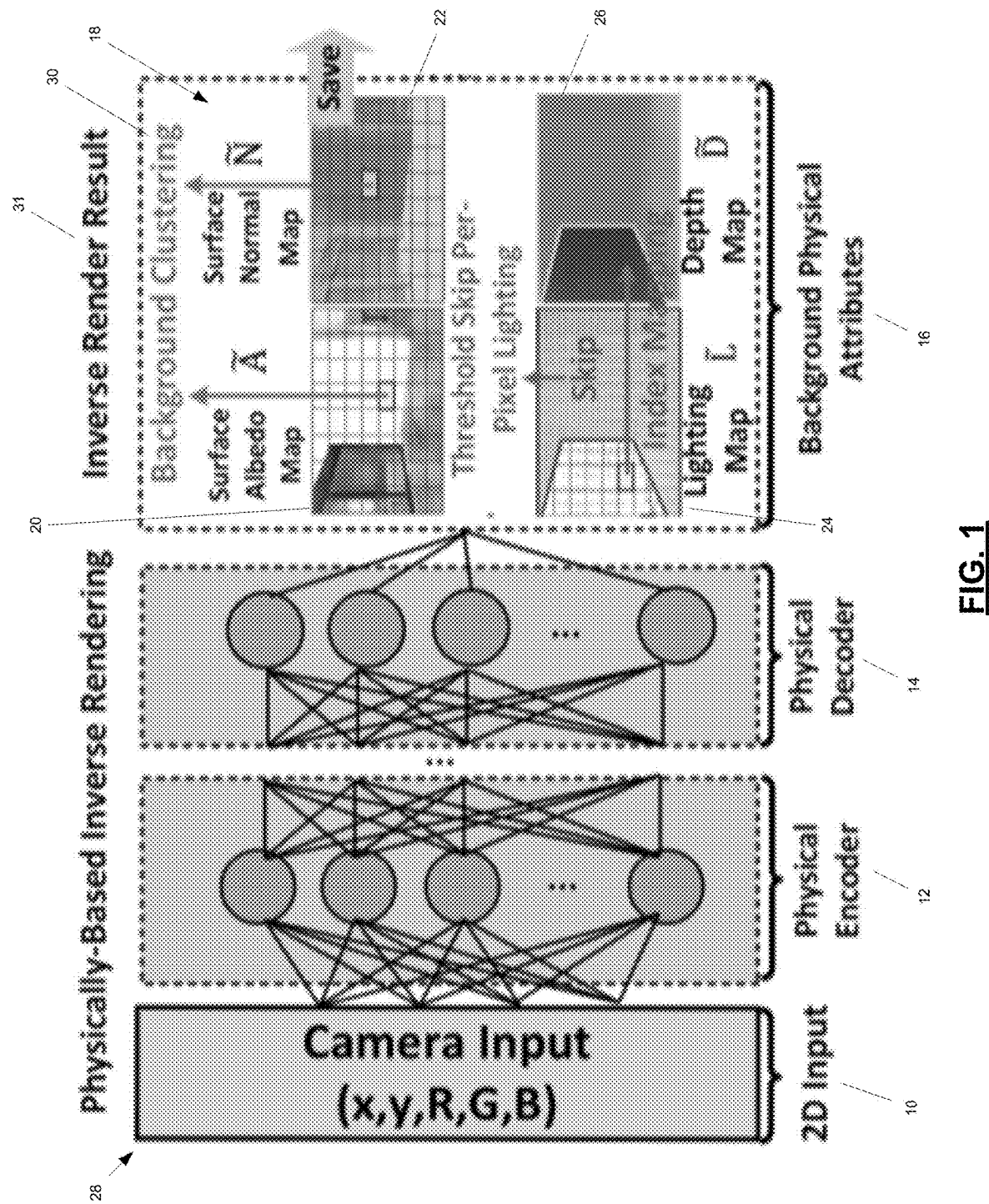
③ Light Transportation Effect

1. Reflection
2. Refraction

④ Shading for Object

1. Diffuse Lighting
2. Specular Lighting
3. Ambient Lighting
4. Shadow

48



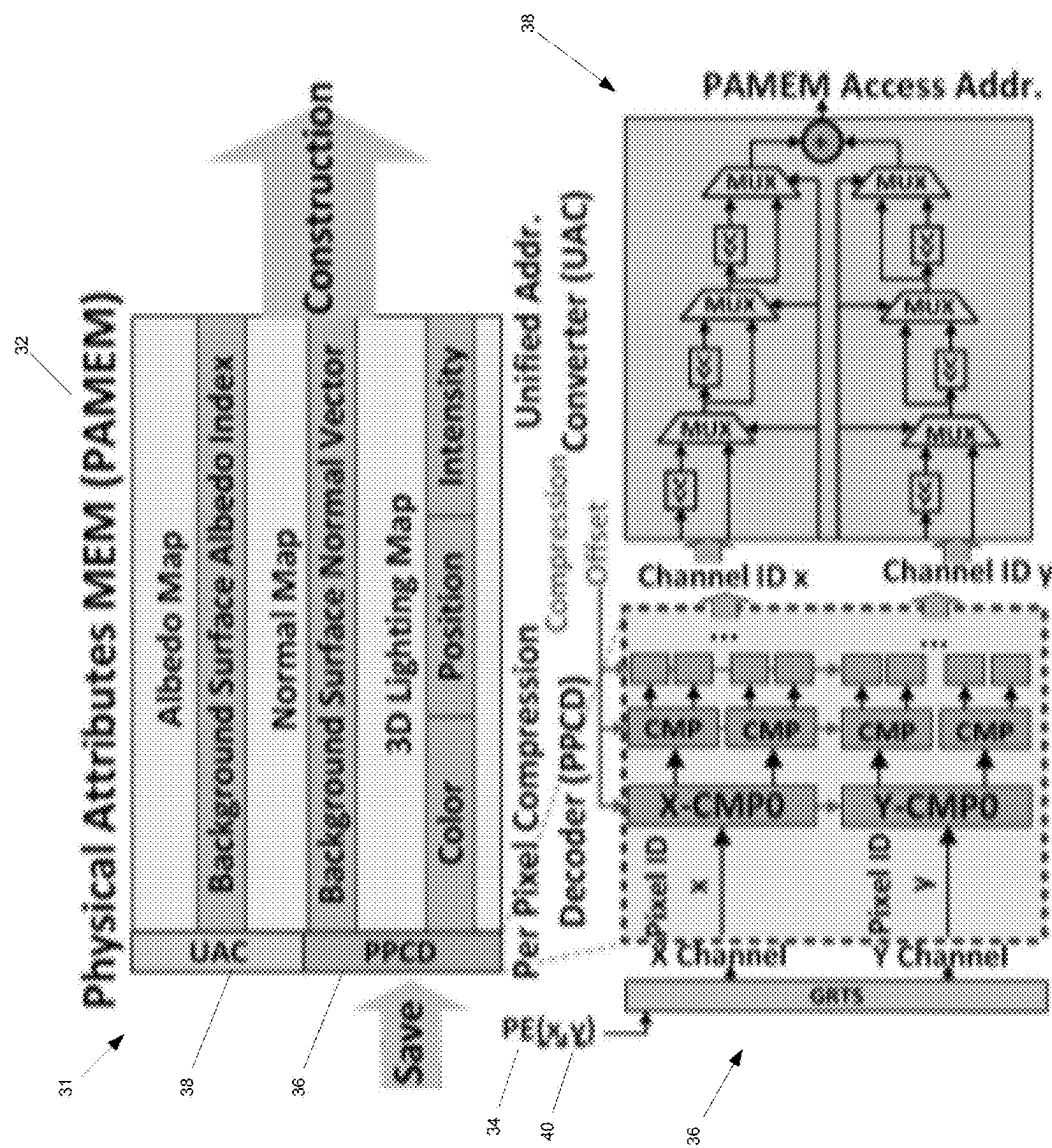


FIG. 2

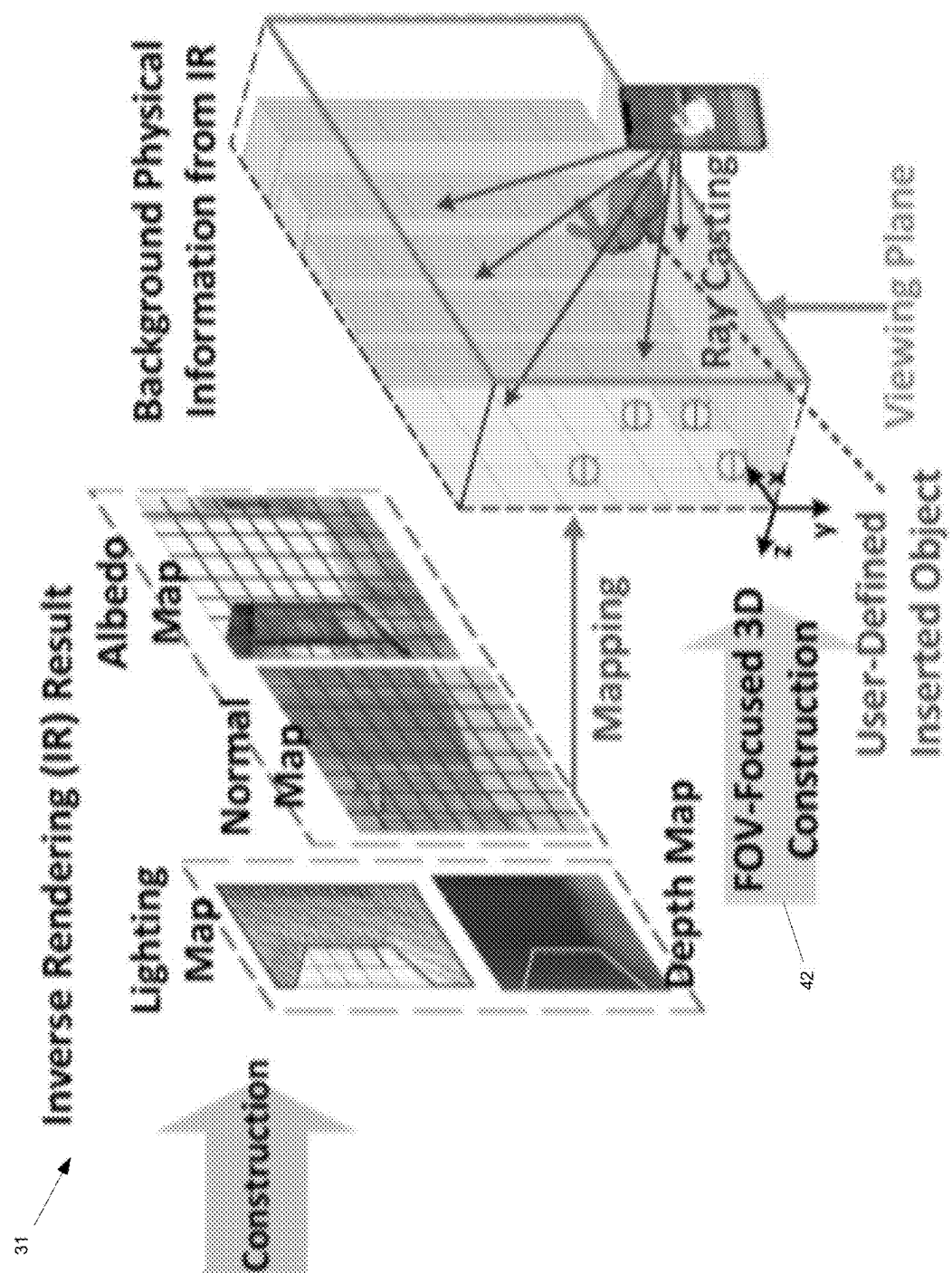
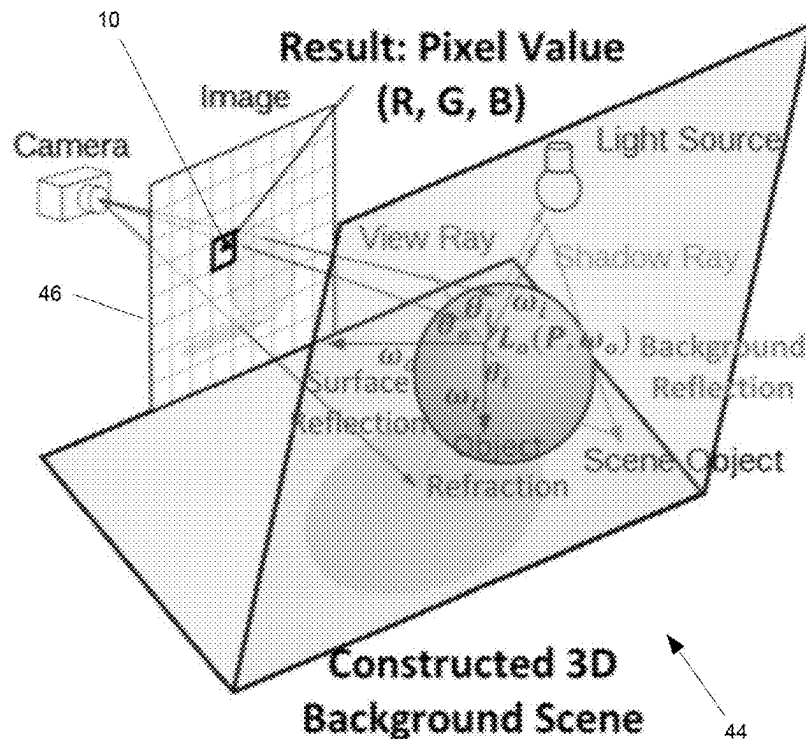
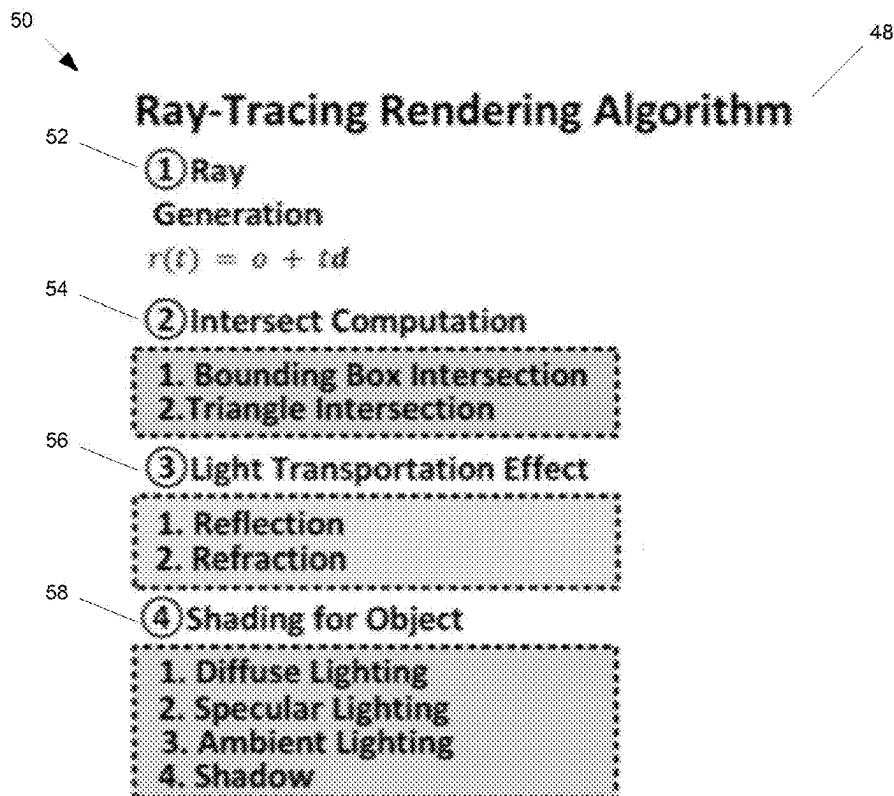
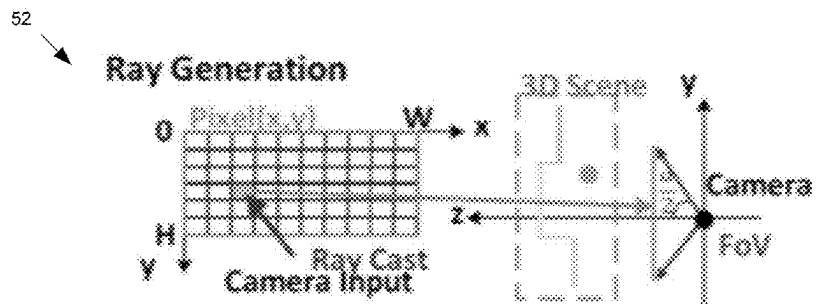
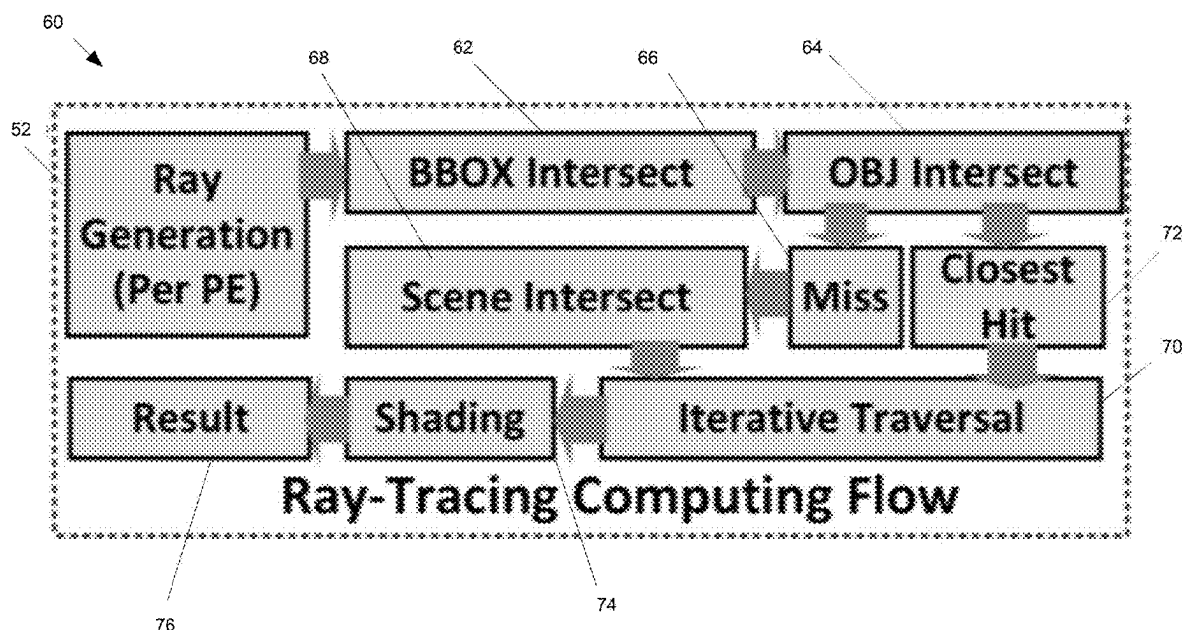


FIG. 3

**FIG. 4****FIG. 5**

**FIG. 6****FIG. 7**

78

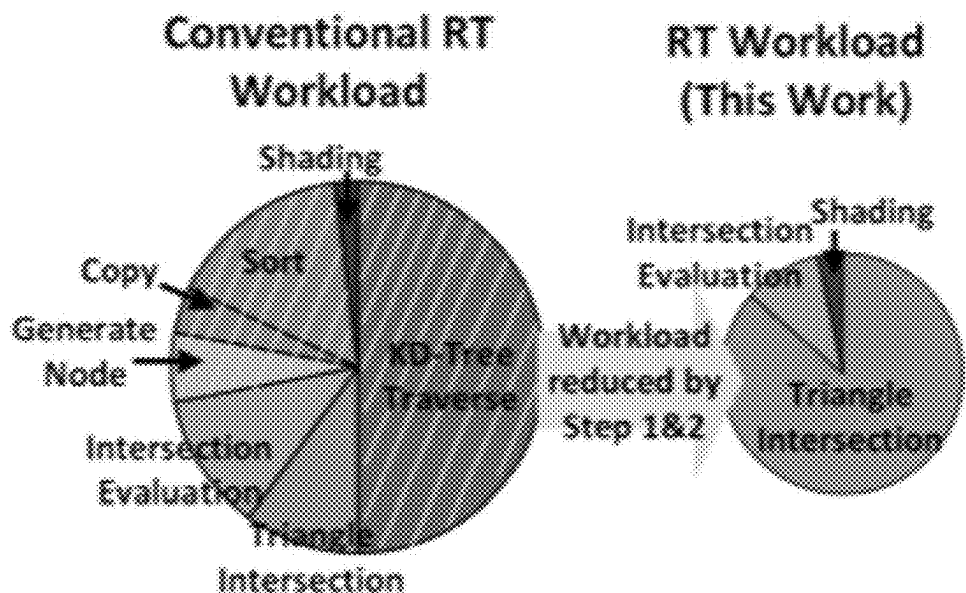


FIG. 8

80

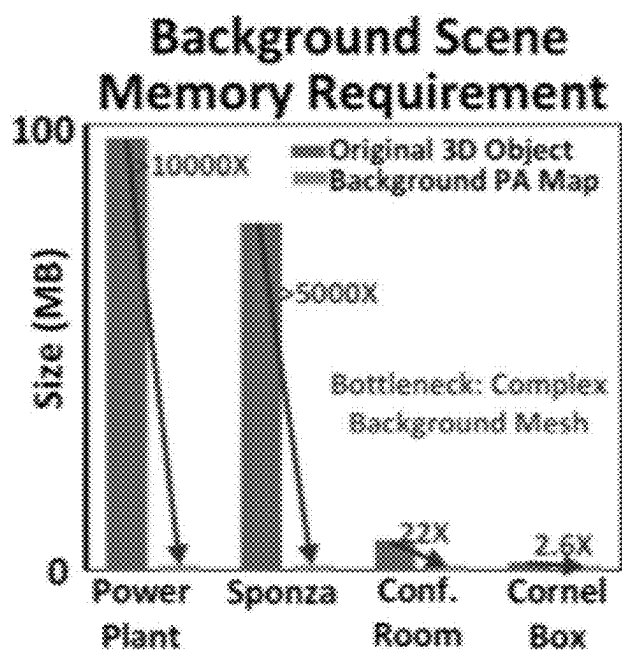


FIG. 9

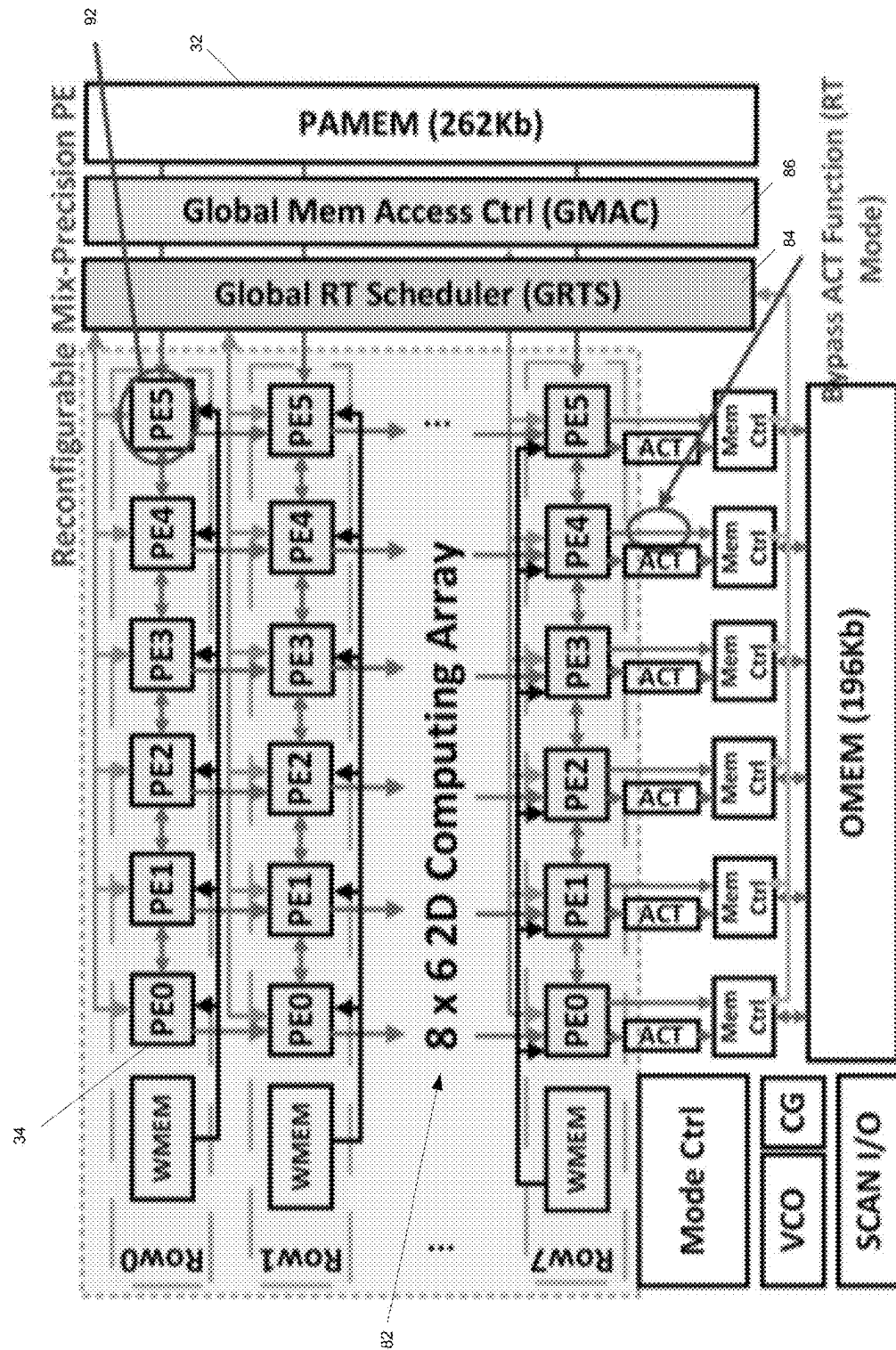


FIG. 10

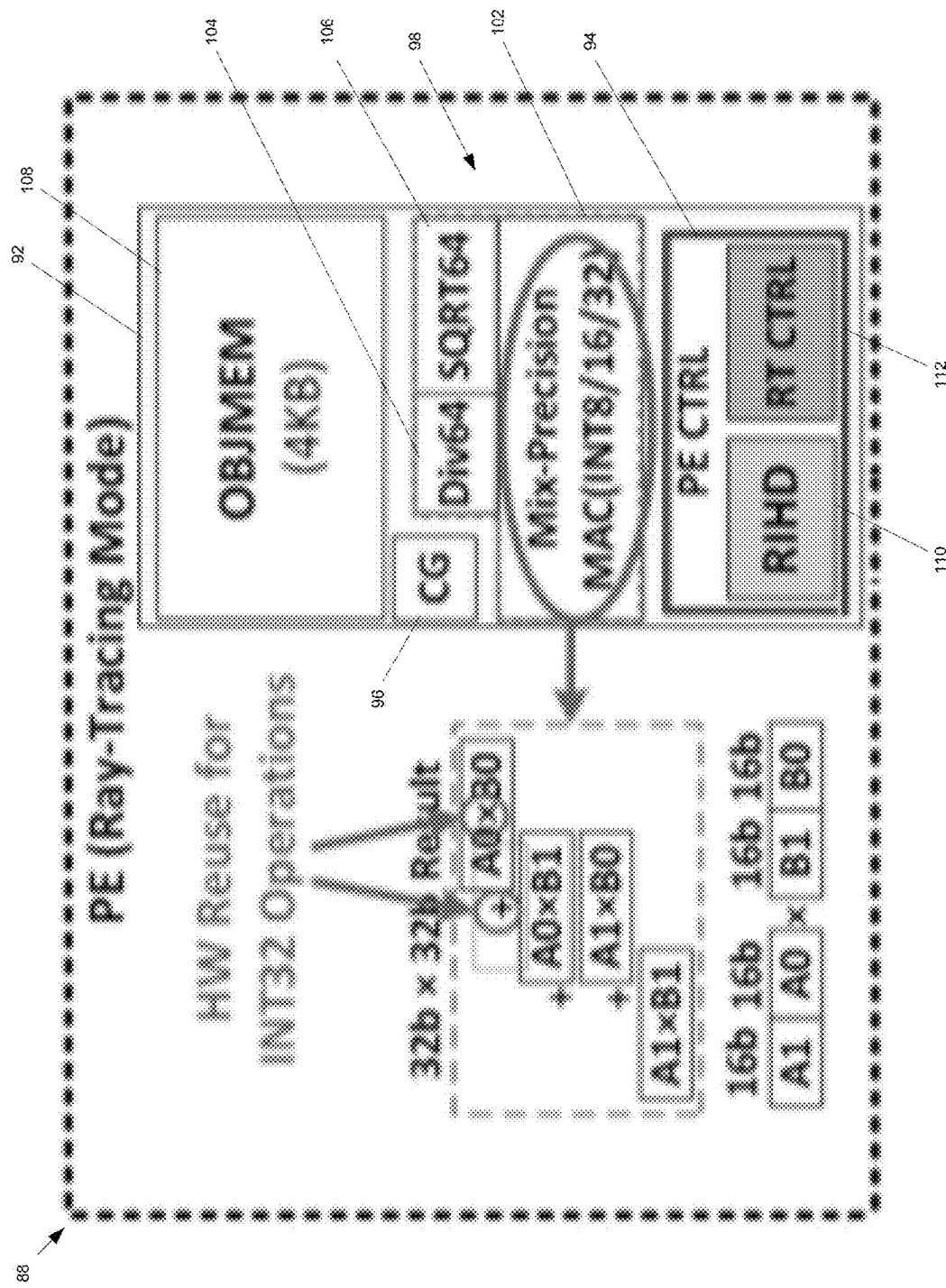


FIG. 11

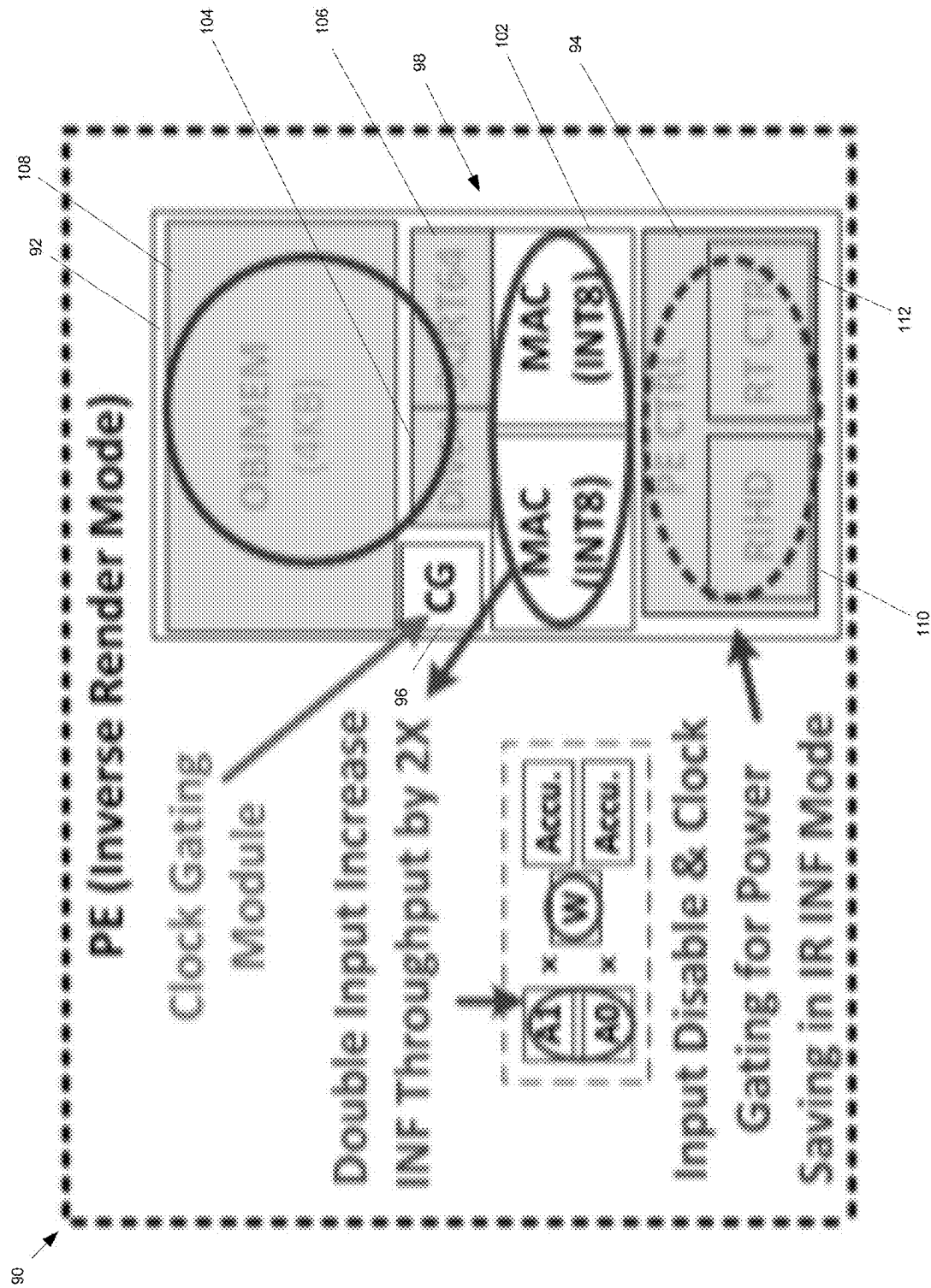


FIG. 12

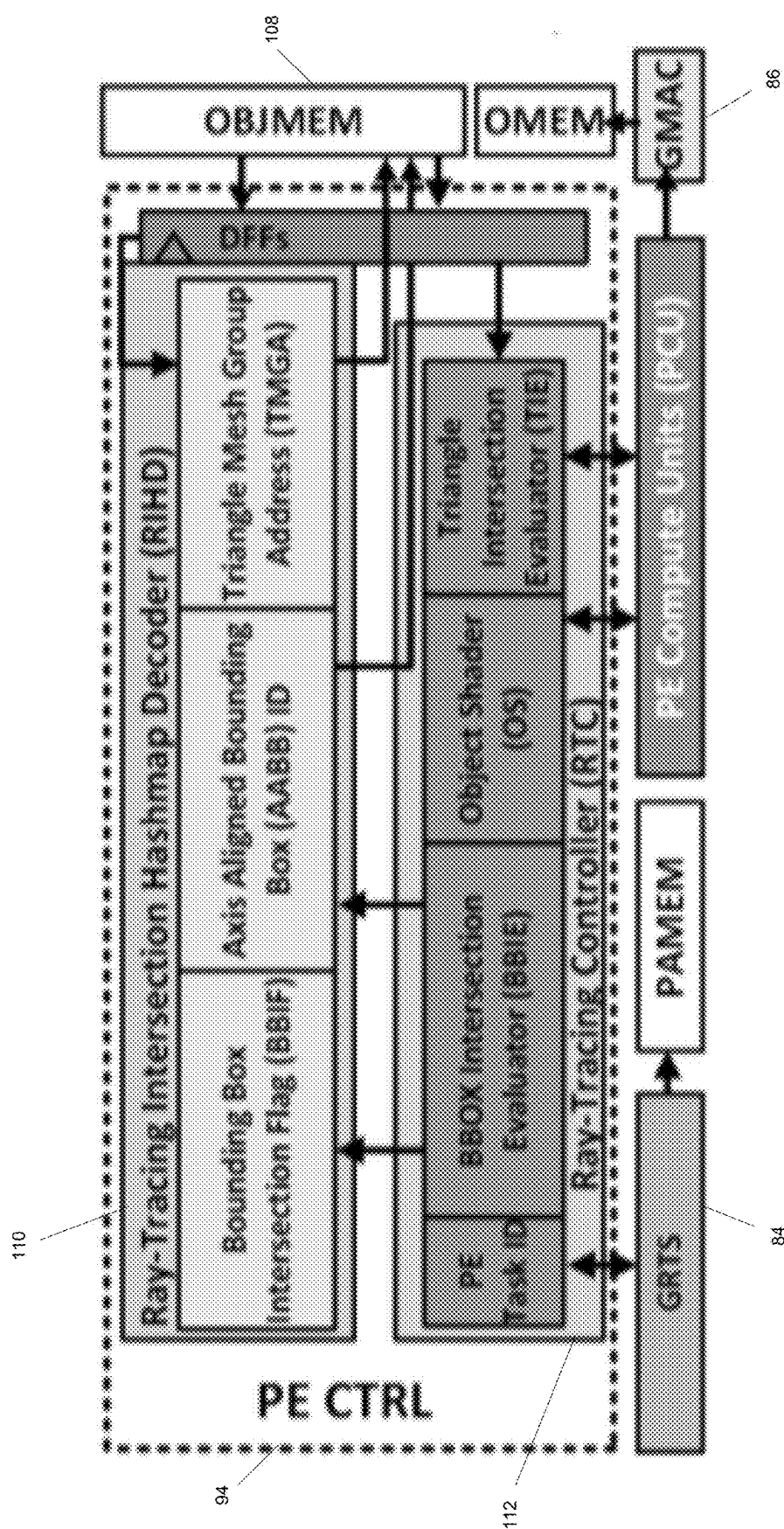


FIG. 13

114

PA Map Memory Saving with Background Clustering

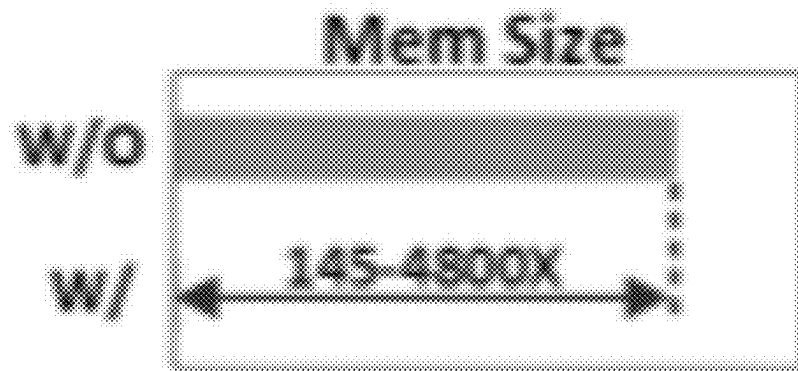


FIG. 14

116

Background Clustering Scheme HW overhead

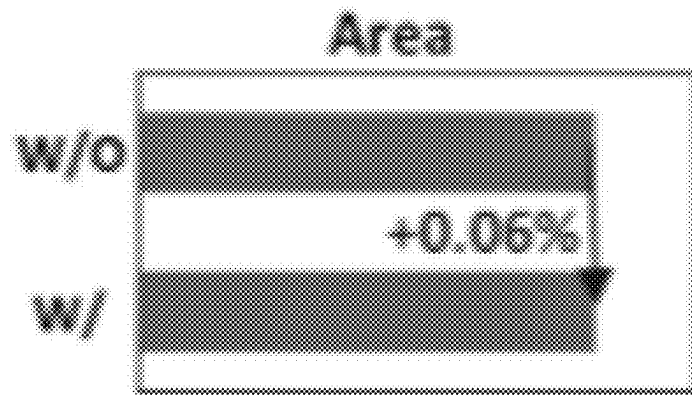


FIG. 15

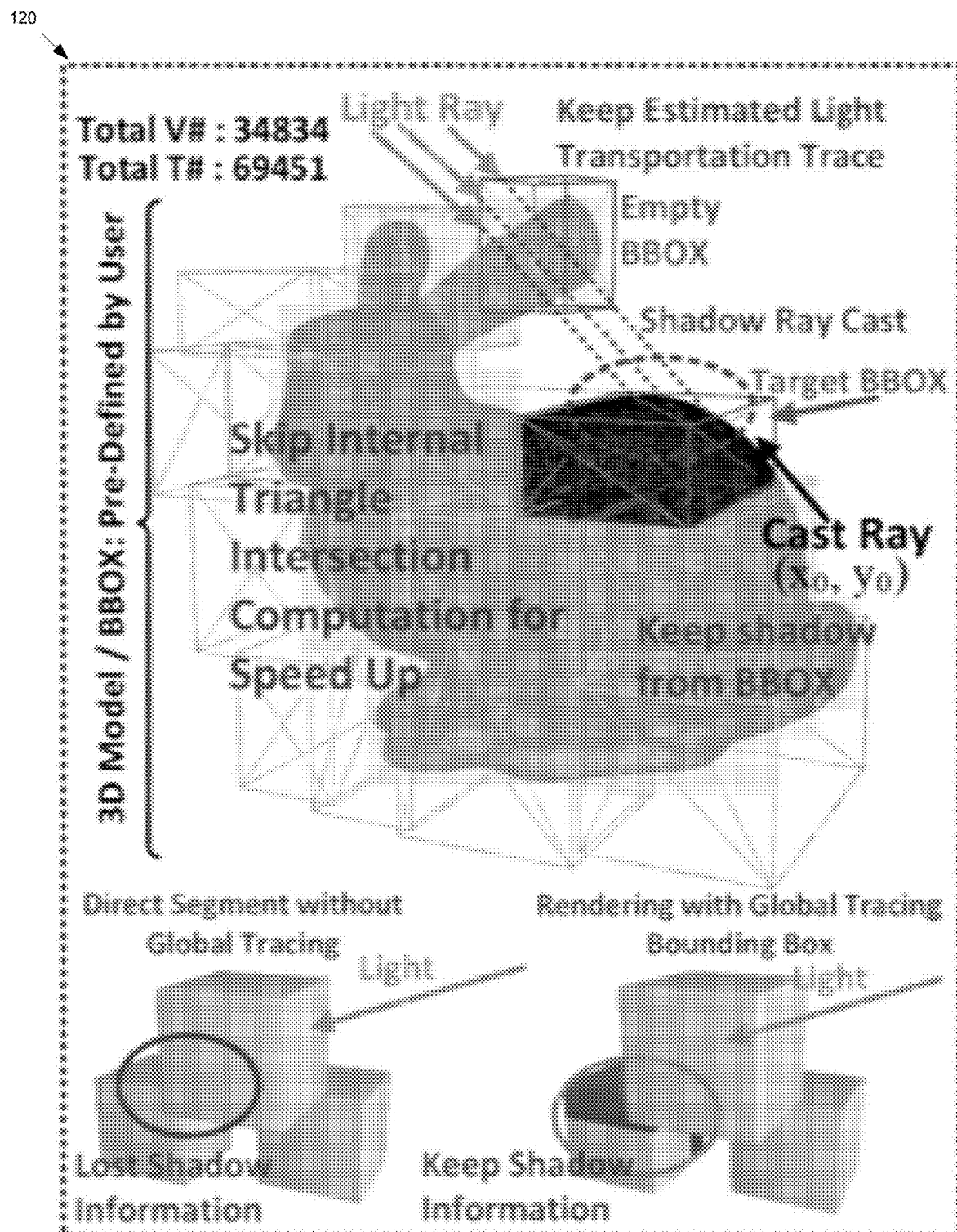


FIG. 16

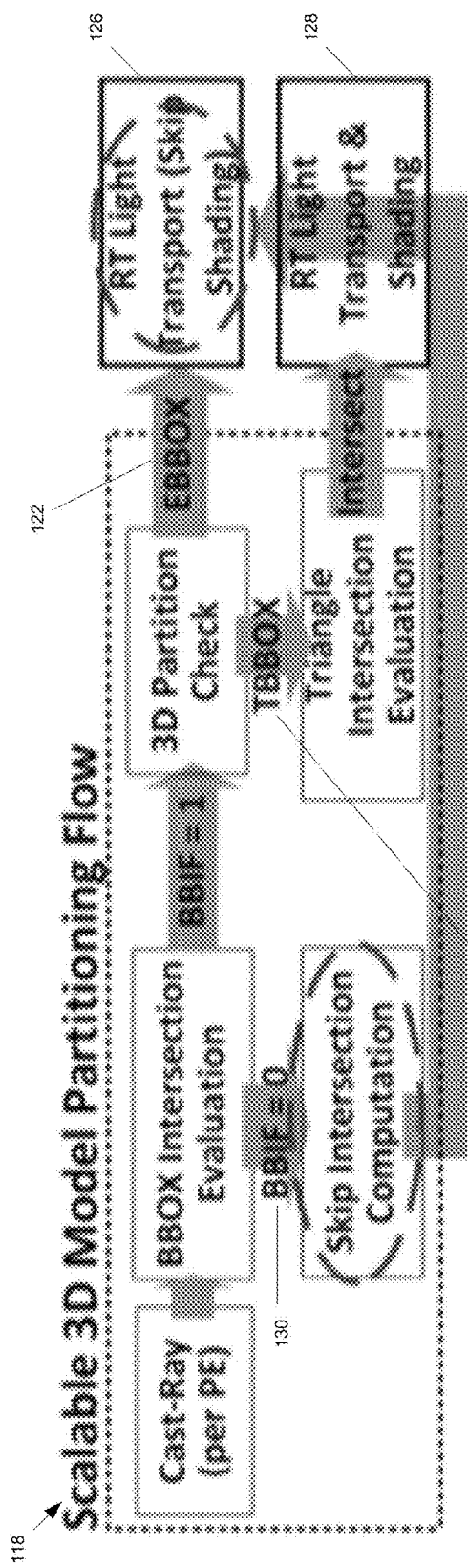


FIG. 17

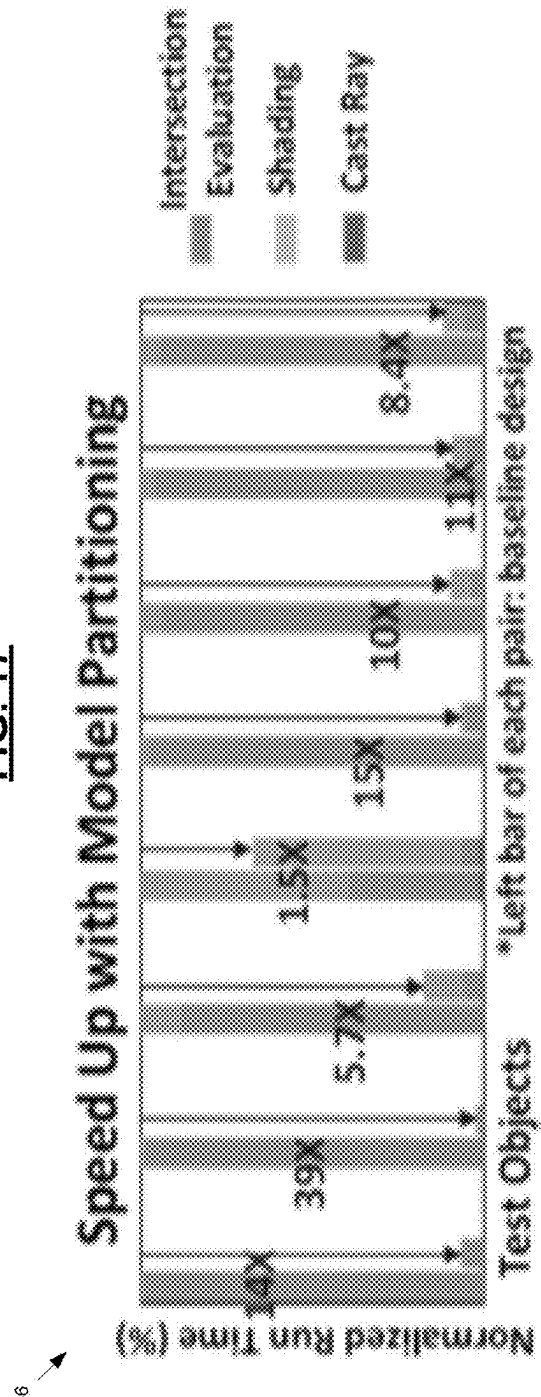


FIG. 18

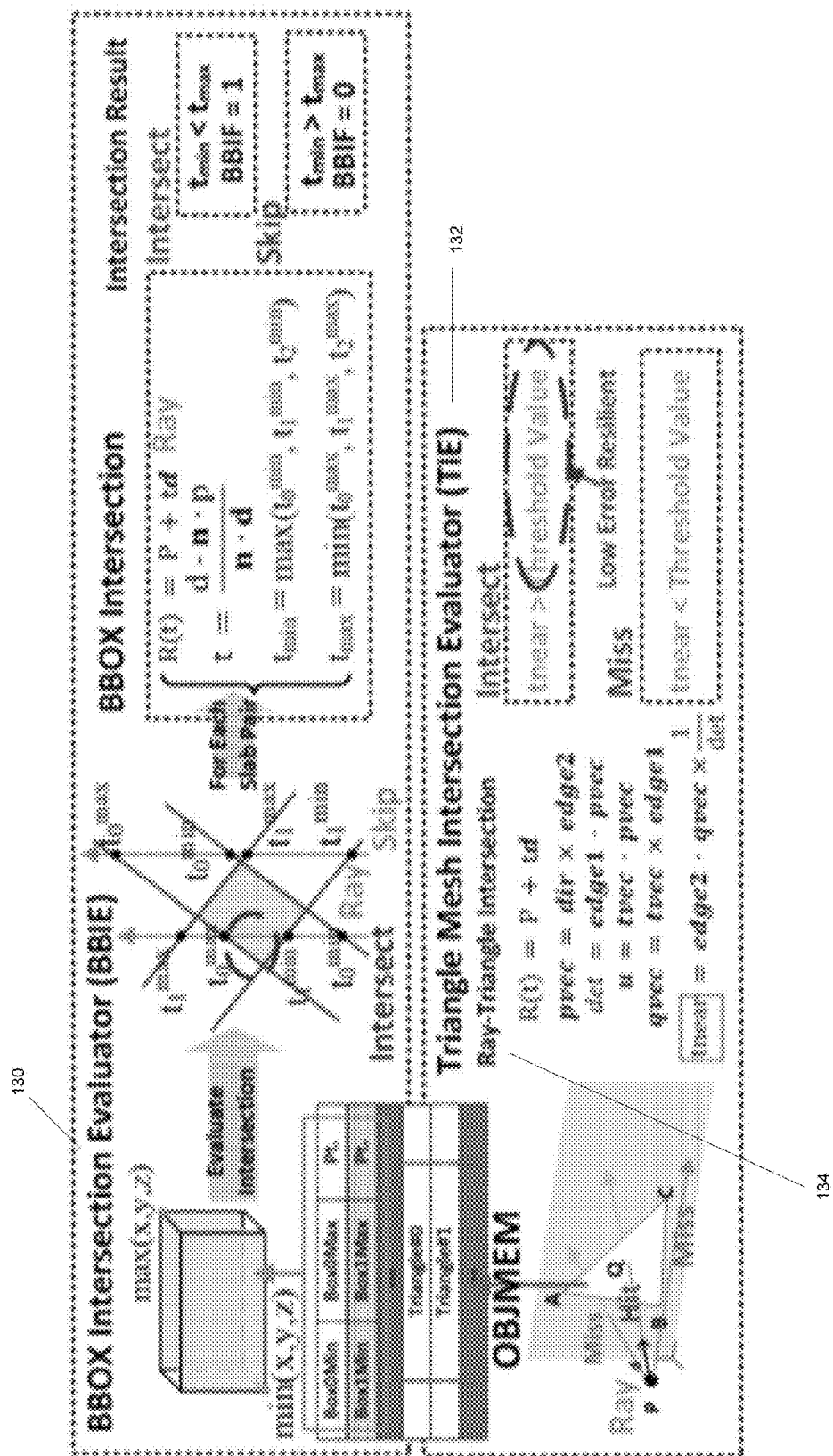


FIG. 19

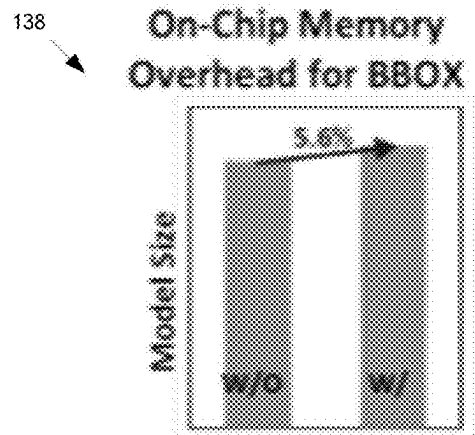


FIG. 20

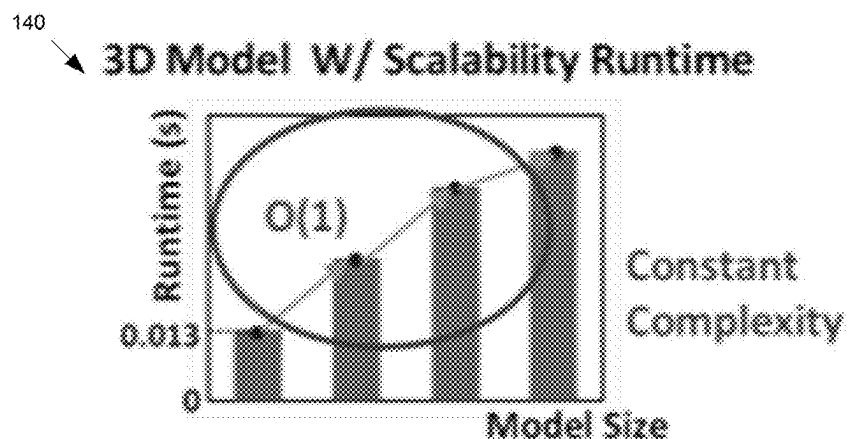


FIG. 21

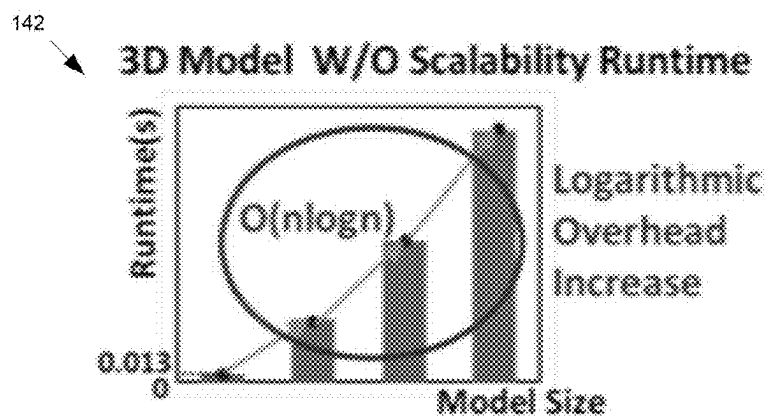


FIG. 22

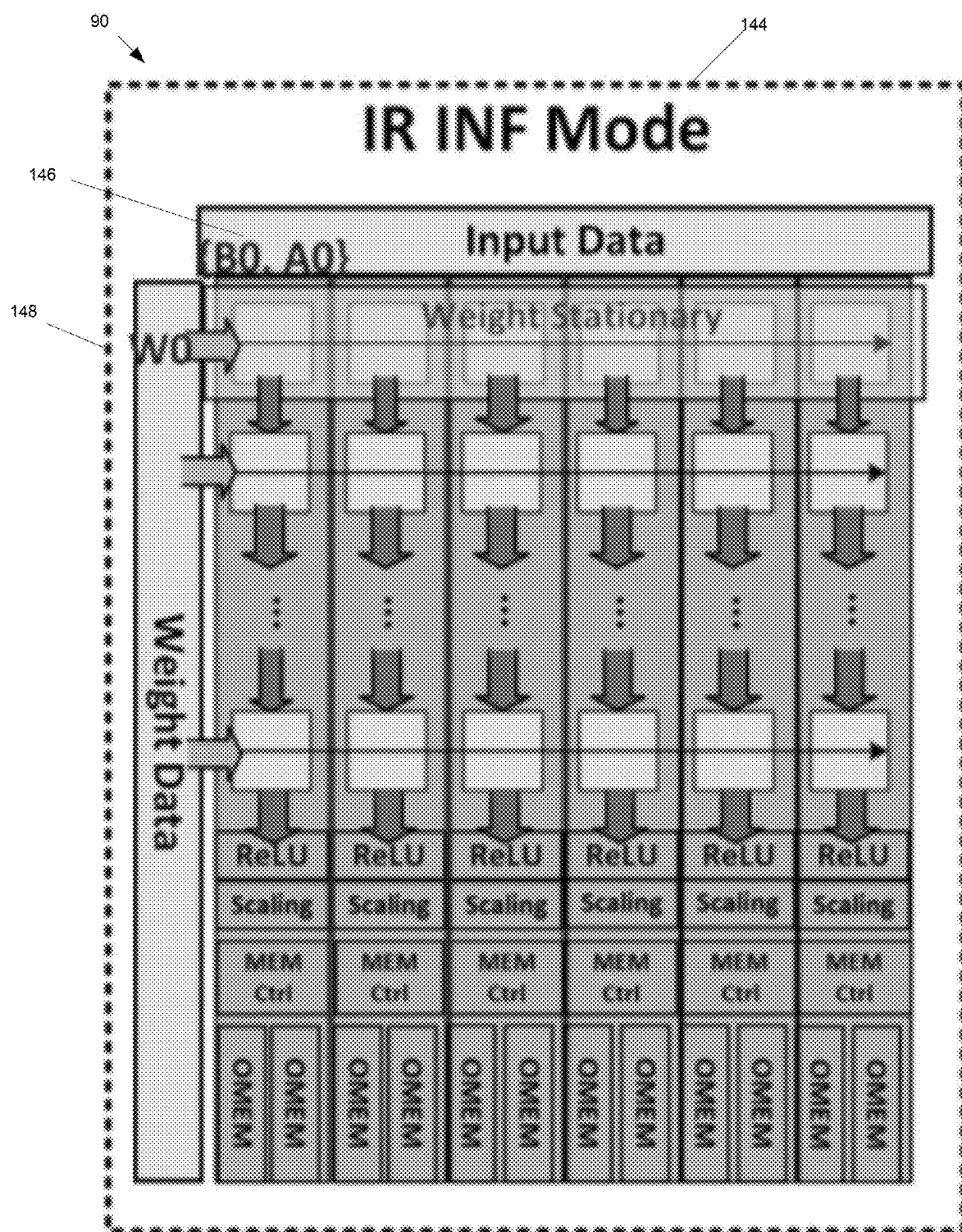


FIG. 23

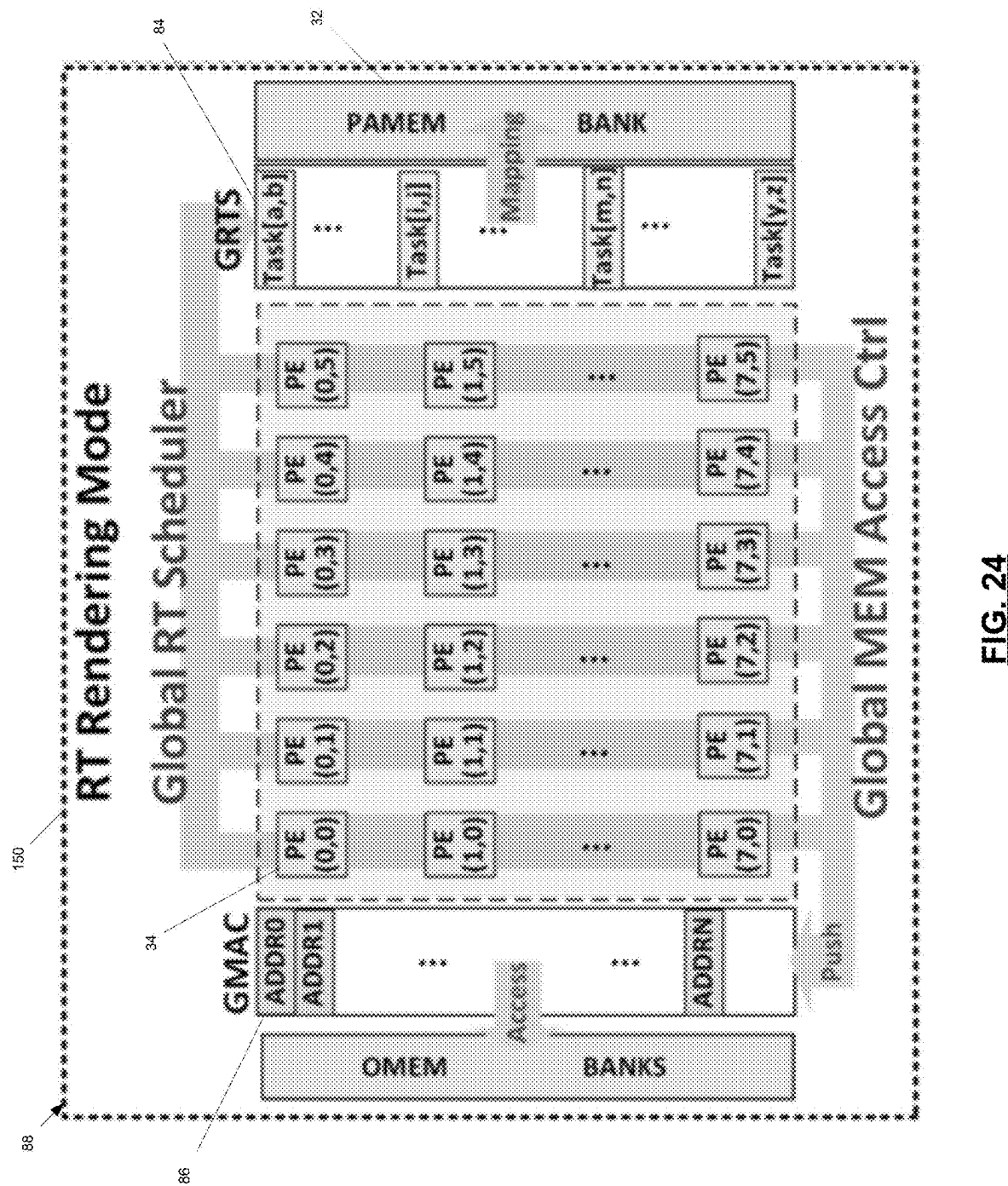


FIG. 24

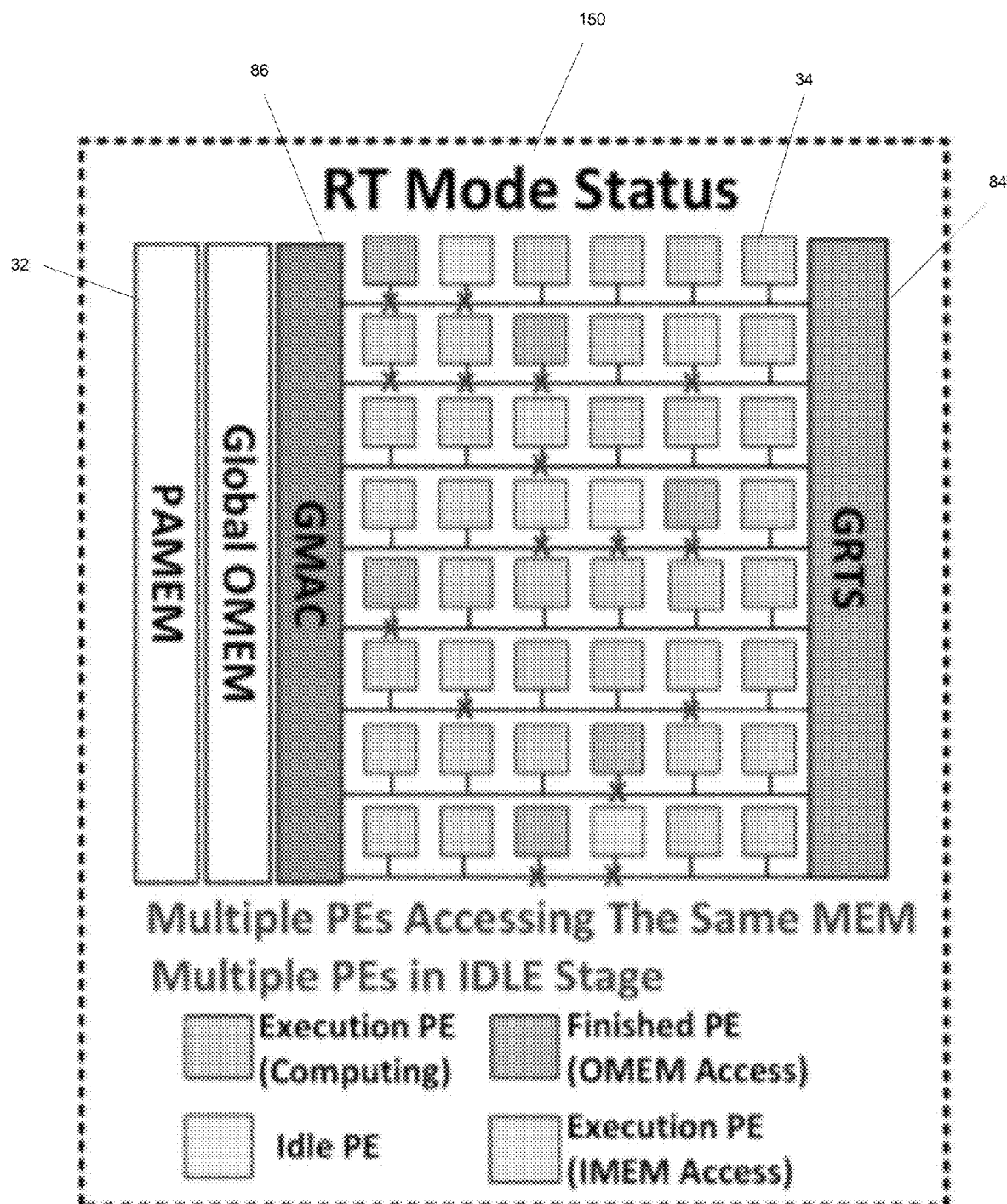


FIG. 25

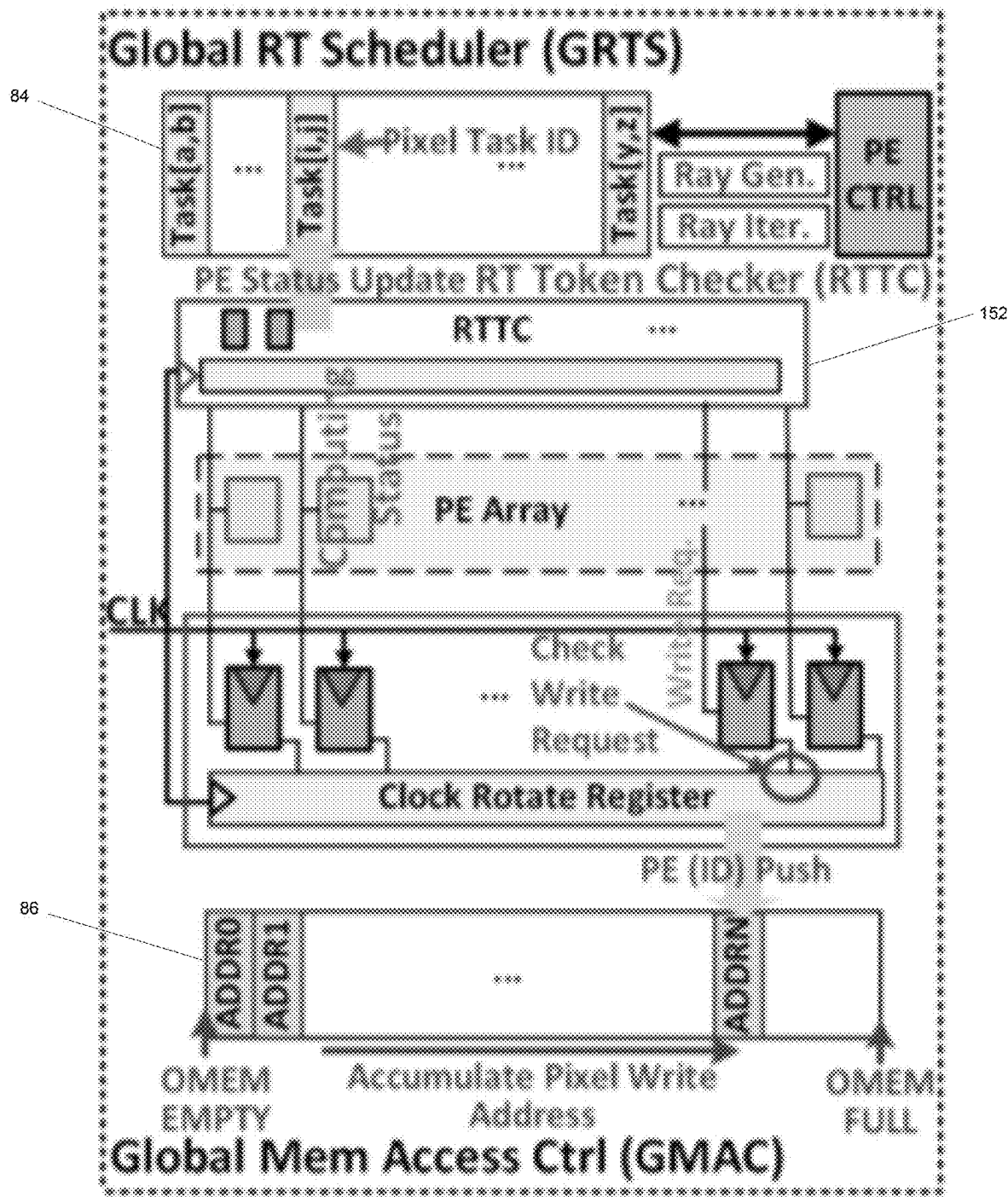


FIG. 26

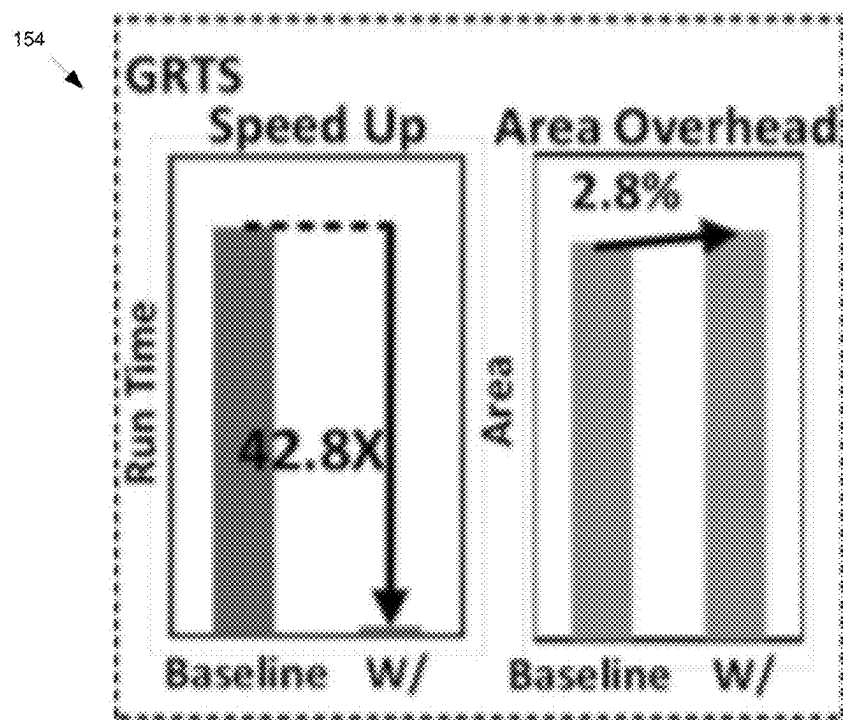


FIG. 27

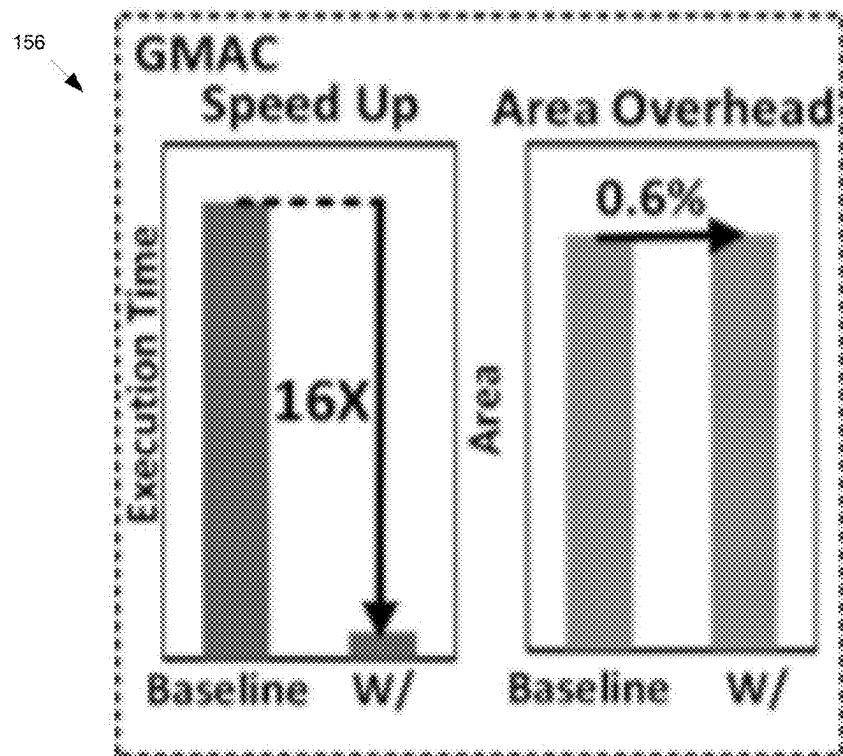
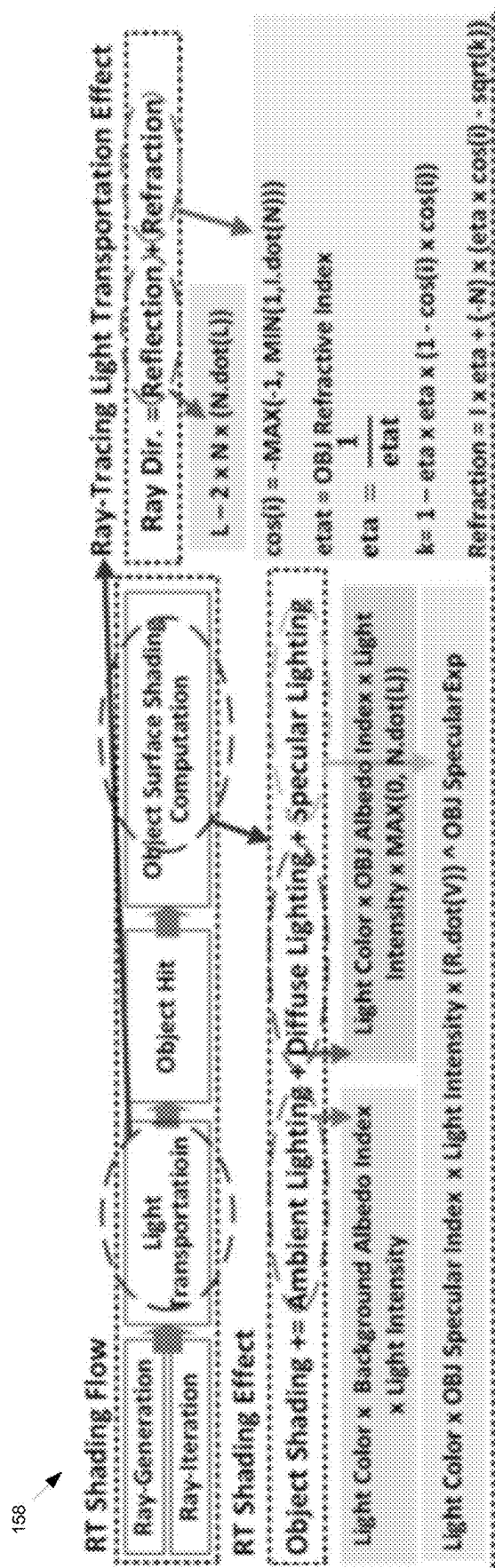


FIG. 28


FIG. 29

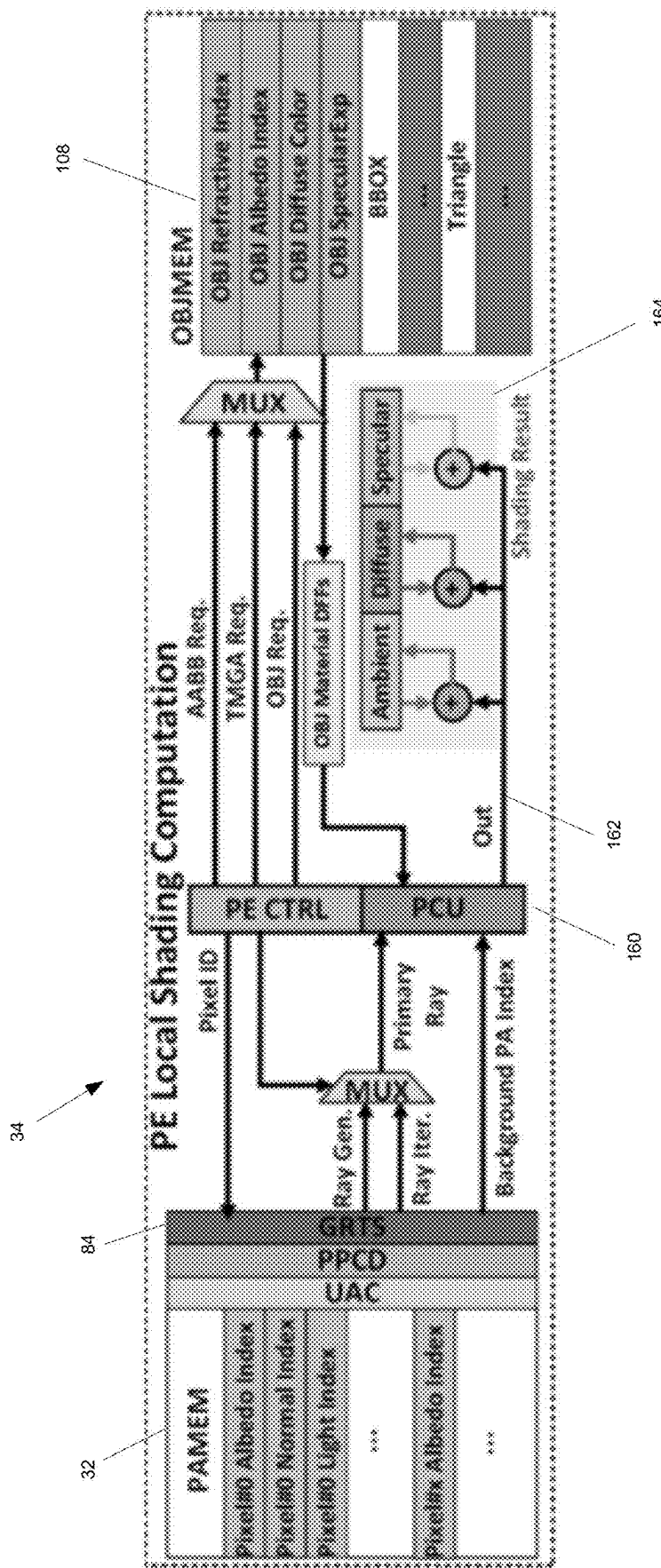


FIG. 30

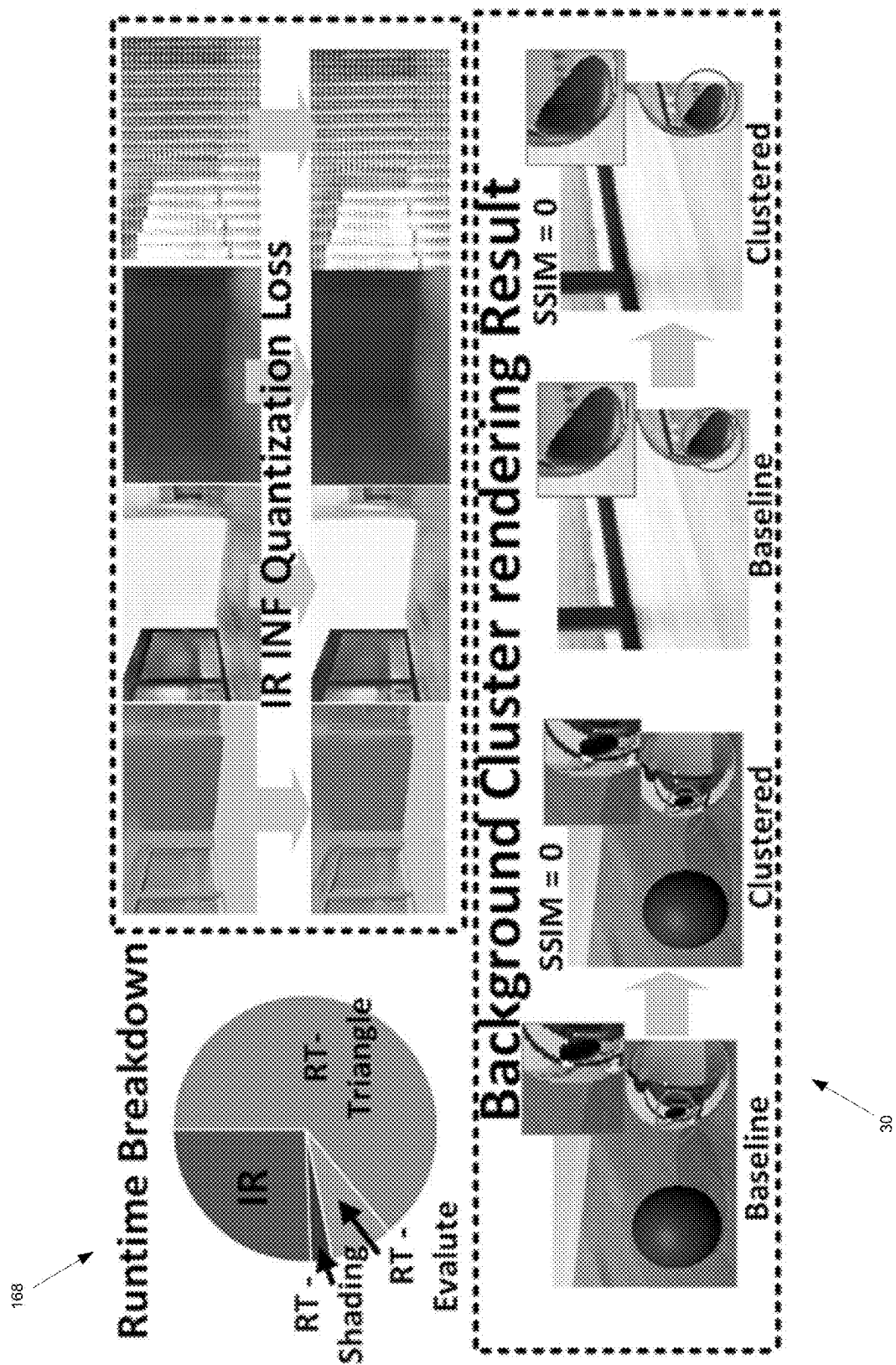


FIG. 31

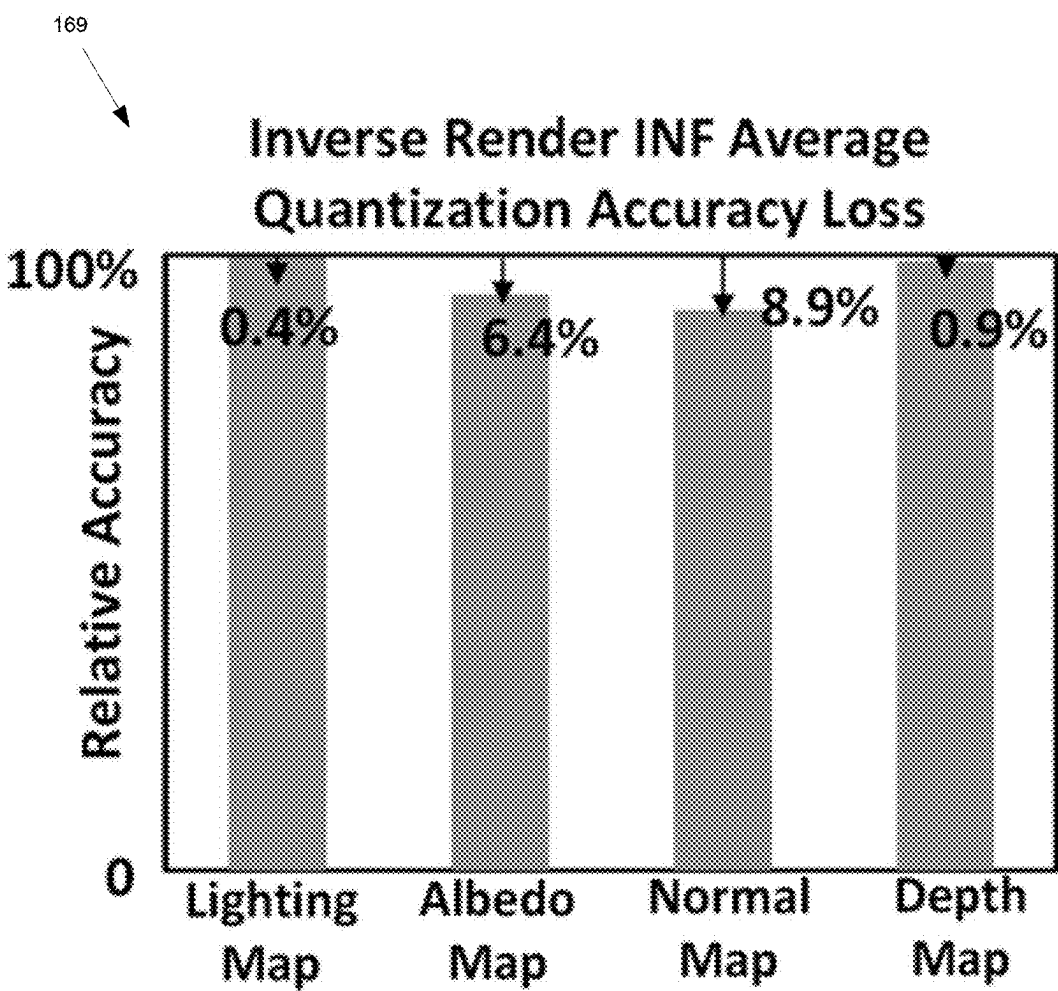


FIG. 32

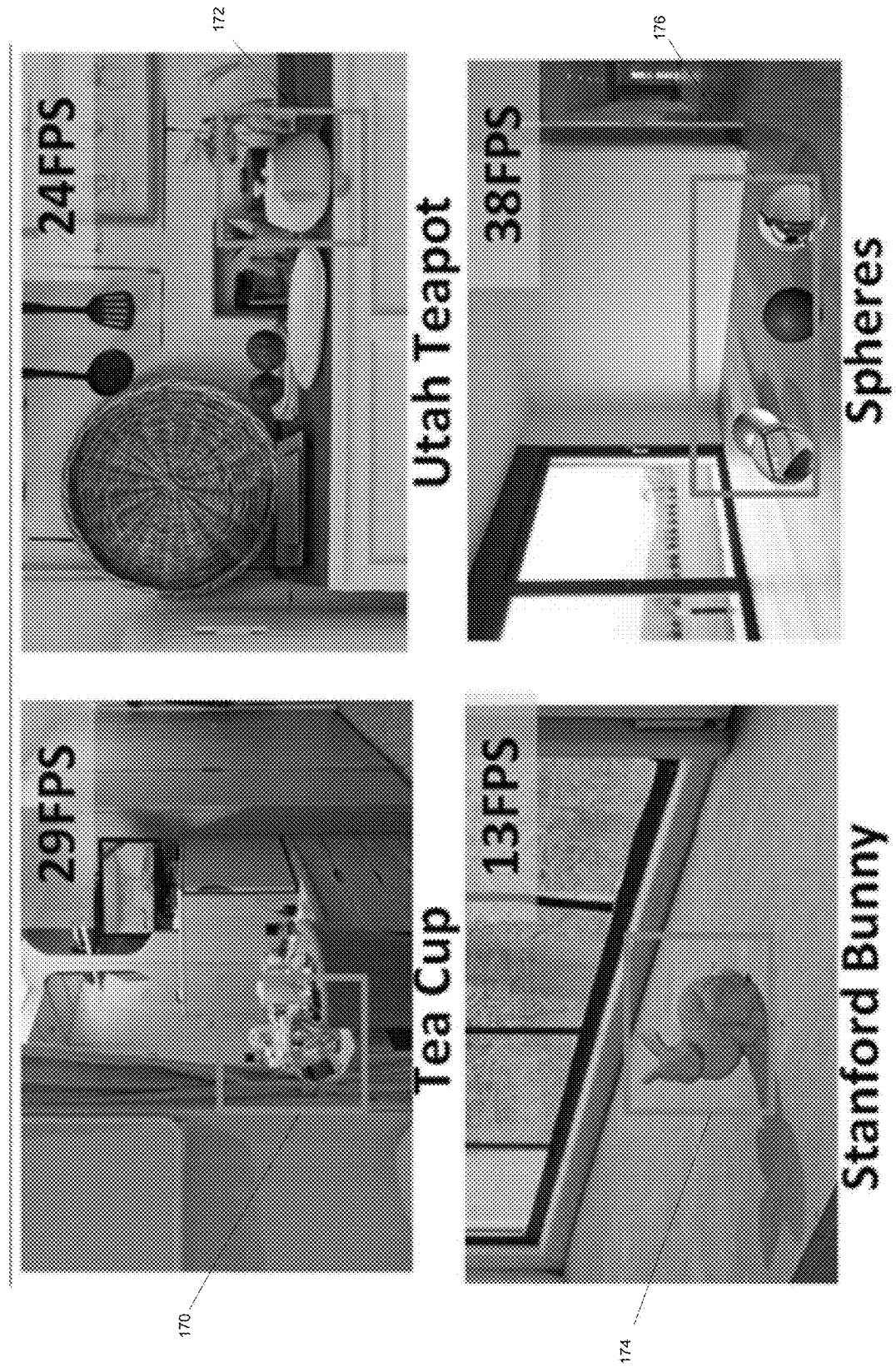


FIG. 33



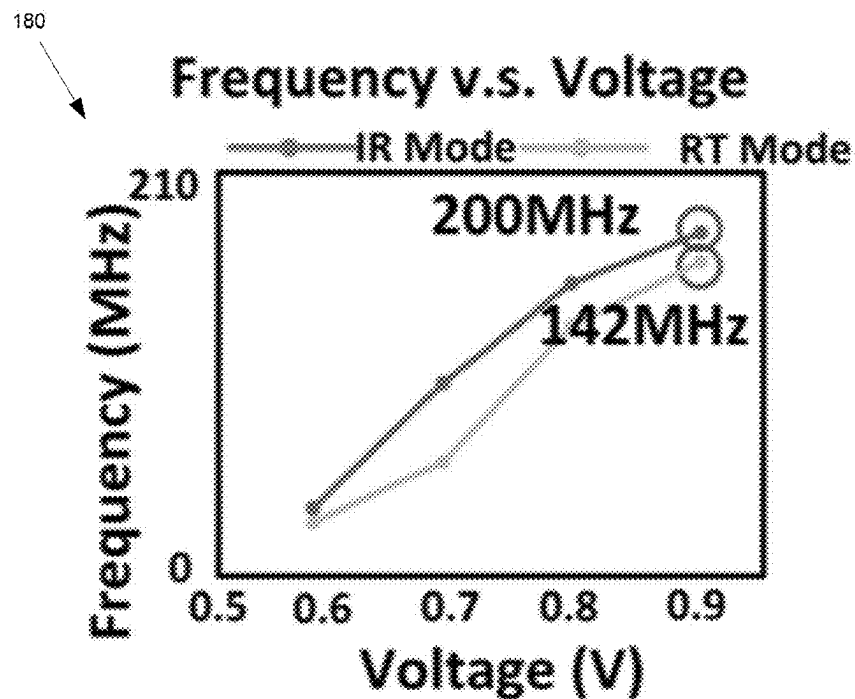


FIG. 35

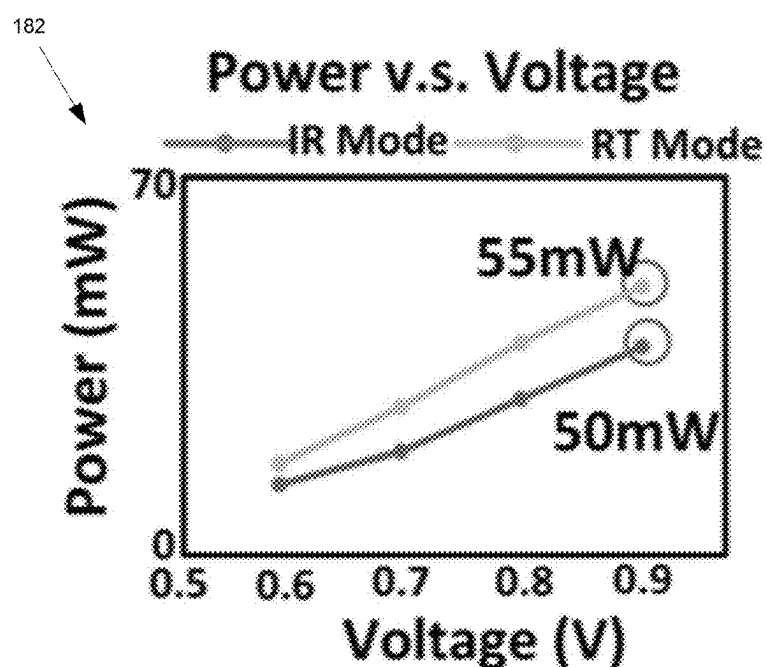


FIG. 36

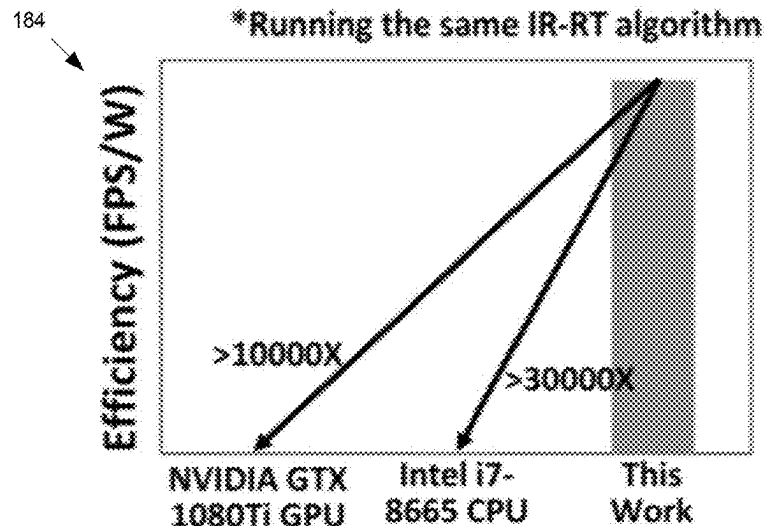


FIG. 37

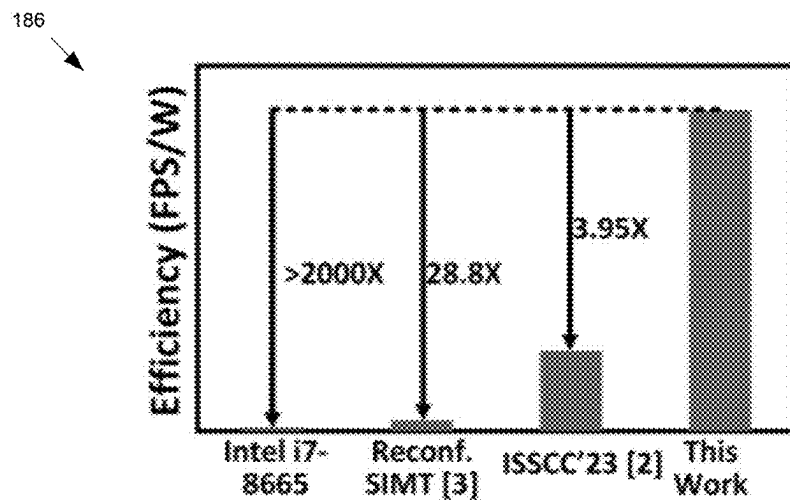


FIG. 38

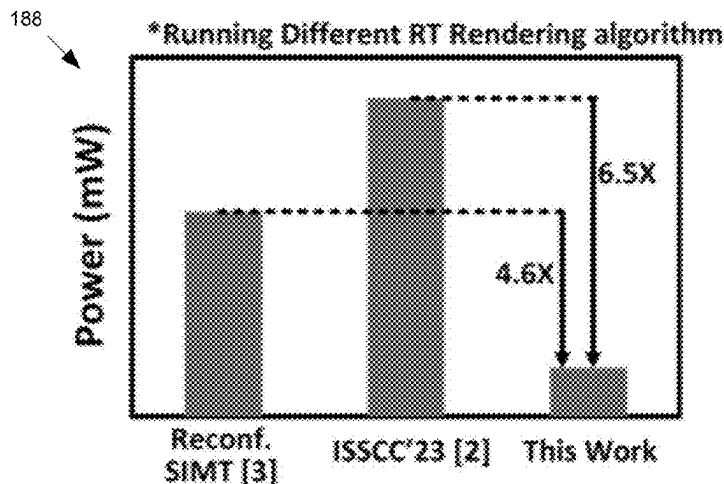


FIG. 39

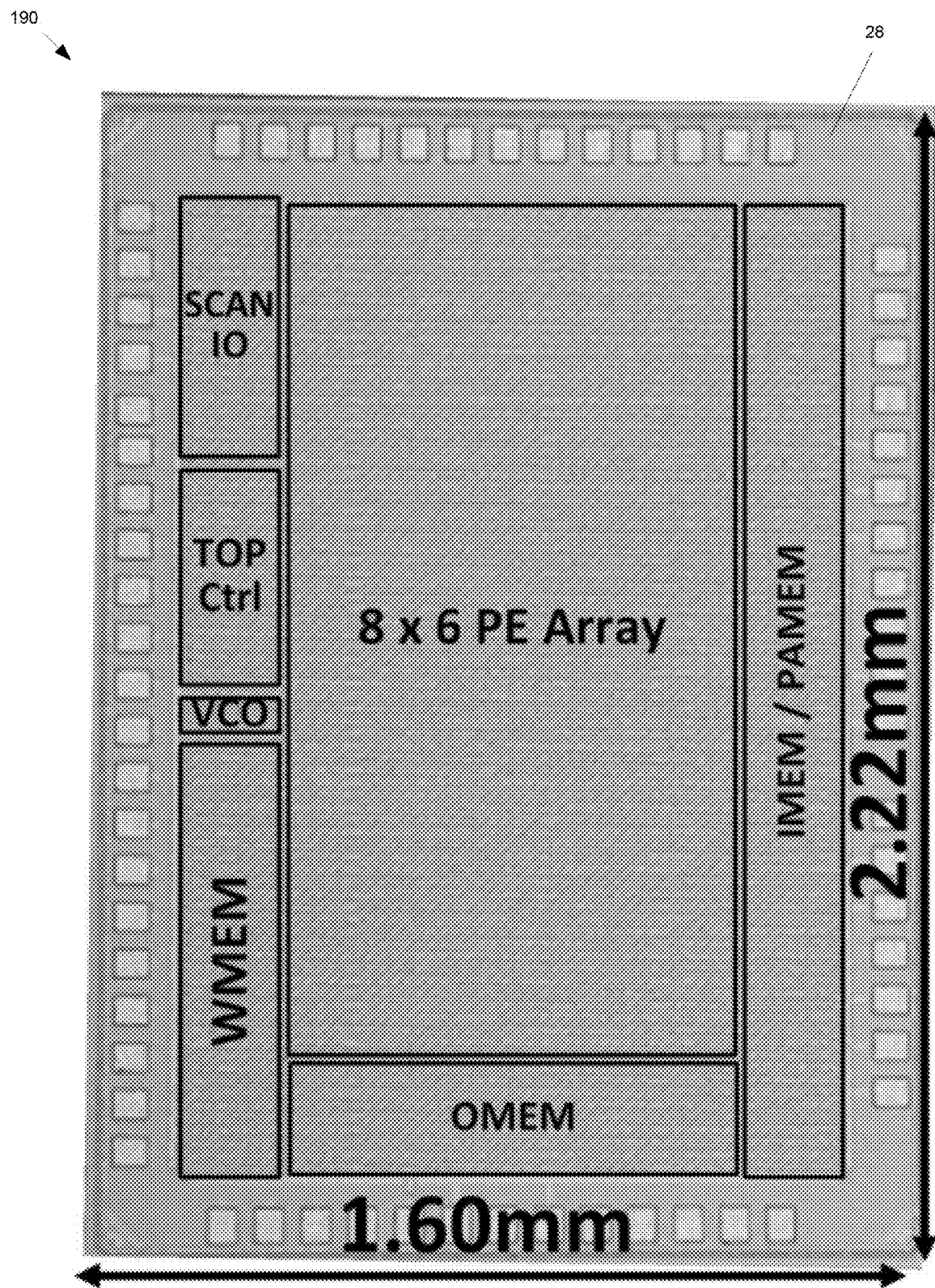


FIG. 40

192

Process	28nm CMOS
Area (mm ²)	3.56mm ²
SRAM	296KB
Supply Vdd	0.6~0.9V
Bit Precision	INT8,16,32,64
Max IR Frequency	200MHz
Max RT Frequency	148MHz
IR Power	40mW @ 0.9V
RT Power	55mW @ 0.9V
IR Efficiency (FPS/W)	500
RT Efficiency (FPS/W)	1418

FIG. 41

EFFICIENT RAY-TRACING RENDERING PROCESSOR WITH OPTIMIZATION FOR MOBILE DEVICES AND SUPPORT OF INVERSE RENDERING

CROSS-REFERENCE TO RELATED APPLICATION

[0001] The present application claims the benefit of priority under 35 U.S.C. § 119 from U.S. Provisional Patent Application Ser. No. 63/553,331 entitled “Efficient Ray-Tracing Rendering Processor with Optimization for Mobile Devices and Support of Inverse Rendering,” filed on Feb. 14, 2024, the disclosure of which is hereby incorporated by reference in its entirety for all purposes.

STATEMENT OF FEDERALLY FUNDED RESEARCH OR SPONSORSHIP

[0002] This invention was made with government support under grant number CCF-2008906 awarded by the National Science Foundation and under grant number A00804302//FA8650-20-2-7009 awarded by the Department of Defense, Department of the Air Force, Air Force Research Laboratory, University of Minnesota. The government has certain rights in the invention.

TECHNICAL FIELD

[0003] The present disclosure generally relates to image generation and insertion, and more specifically relates to efficient ray-tracing rendering processors with optimization for mobile devices and support of inverse rendering.

BACKGROUND

[0004] As the applications of Augmented Reality (AR) or Virtual Reality (VR) expand rapidly with the growing demands on enhanced visual realism, photorealistic image generation and insertion has become an essential feature for the emerging AR applications providing real-time workplace/household visual assistance. Physically Based Ray-Tracing (PBRT) is often used where synthesized images are generated by simulating the real environment and tracing the light transportation to achieve photorealistic effects, such as reflection, refraction, soft shadows, etc. PBRT is widely used in product design, medical visualization, video games and movie effects. To enable photorealistic rendering, there is a strong demand to support ray-tracing (RT) on mobile devices. However, the challenges are: (1) unstructured memory access pattern and complex control flow lead to scheduling difficulty; (2) high memory requirements exhaust the limited SRAM space on edge devices; (3) low error tolerance requires high precision for computing; (4) complex computations, such as division and square root, require significant computing resources for the edge devices. As a result, common rendering engines are mainly based on the lower cost rasterization rendering technique. Unfortunately, rasterization rendering fails to produce photorealistic synthesis. Few ASICs have been fabricated so far as a mobile RT solution.

[0005] The description provided in the background section should not be assumed to be prior art merely because it is mentioned in or associated with the background section. The background section may include information that describes one or more aspects of the subject technology.

BRIEF DESCRIPTION OF DRAWINGS

[0006] The disclosure is better understood with reference to the following drawings and description. The elements in the figures are not necessarily to scale, emphasis instead being placed upon illustrating the principles of the disclosure. Moreover, in the figures, like-referenced numerals may designate to corresponding parts throughout the different views.

[0007] FIG. 1 is a schematic diagram illustrating physically-based inverse rendering, according to certain aspects of the present disclosure.

[0008] FIG. 2 is a schematic diagram illustrating a physical attributes MEM (PAMEM) utilized in the physically-based inverse rendering of FIG. 1, according to certain aspects of the present disclosure.

[0009] FIG. 3 is a schematic diagram illustrating an inverse rendering result of the physically-based inverse rendering of FIG. 1, according to certain aspects of the present disclosure.

[0010] FIG. 4 illustrates a constructed 3D background scene, according to certain aspects of the present disclosure.

[0011] FIG. 5 illustrates a flow of a ray-tracing rendering algorithm, according to certain aspects of the present disclosure.

[0012] FIG. 6 illustrates a flow of a ray generation of the ray-tracing rendering algorithm of FIG. 5, according to certain aspects of the present disclosure.

[0013] FIG. 7 illustrates an example ray-tracing computing flow, according to certain aspects of the present disclosure.

[0014] FIG. 8 schematically illustrates comparison charts for comparing conventional RT workload versus RT workload of the present disclosure.

[0015] FIG. 9 illustrates a background scene memory requirement chart.

[0016] FIG. 10 illustrates the top-level architecture of the disclosed technology.

[0017] FIG. 11 schematically illustrates a ray-tracing mode in a PE, according to certain aspects of the present disclosure.

[0018] FIG. 12 schematically illustrates an inverse rendering mode in a PE, according to certain aspects of the present disclosure.

[0019] FIG. 13 illustrates a local PE Controller of each reconfigurable mixed-precision PE, according to certain aspects of the present disclosure.

[0020] FIG. 14 is a diagram illustrating PA map memory saving with background clustering by mem size.

[0021] FIG. 15 is a diagram illustrating background clustering scheme HW overhead by area.

[0022] FIG. 16 is a schematic diagram depicting a scalable 3D model partitioning flow, in RT mode, according to certain aspects of the present disclosure.

[0023] FIG. 17 is a block diagram depicting a scalable 3D model partitioning flow, in RT mode, according to certain aspects of the present disclosure.

[0024] FIG. 18 chart 136 illustrating normalized run time in percentage versus intersection evaluation, shading, and cast ray for test objects.

[0025] FIG. 19 is a schematic diagram illustrating a BBOX intersection evaluator, according to certain aspects of the present disclosure.

[0026] FIG. 20 is a chart depicting model size versus memory overhead.

[0027] FIG. 21 is a chart depicting runtime in seconds versus model size for a 3D model with scalability runtime.

[0028] FIG. 22 is a chart depicting runtime in seconds versus model size for a 3D model without scalability runtime.

[0029] FIG. 23 depicts on-chip data movement on the chip in the IR mode, according to certain aspects of the present disclosure.

[0030] FIG. 24 depicts on-chip data movement on the chip in the RT mode, according to certain aspects of the present disclosure.

[0031] FIG. 25 illustrates multiple PEs having memory access conflicts in RT status mode, according to certain aspects of the present disclosure.

[0032] FIG. 26 illustrates a global RT scheduler (GRTS), according to certain aspects of the present disclosure.

[0033] FIG. 27 is a chart depicting 42.8 \times overall speed up from the GRTS.

[0034] FIG. 28 is a chart depicting 16 \times overall speed up from the GMAC.

[0035] FIG. 29 is a schematic diagram illustrating RT shading flow, according to certain aspects of the present disclosure.

[0036] FIG. 30 is a schematic diagram illustrating PE local shading computation, according to certain aspects of the present disclosure.

[0037] FIG. 31 is schematic diagram illustrating the total runtime breakdown for the IR-RT flow and demonstrates the background clustering scheme, according to certain aspects of the present disclosure.

[0038] FIG. 32 is a chart depicting relative accuracy for the lighting map, the surface albedo map, the surface normal map, and the depth map.

[0039] FIG. 33 illustrates virtual object insertion examples using the IR-RT rendering scheme, according to certain aspects of the present disclosure.

[0040] FIG. 34 is a schematic diagram depicting photorealistic effects of refraction, reflection and object shadow, according to certain aspects of the present disclosure.

[0041] FIG. 35 is a chart depicting frequency versus voltage with a supply voltage from 0.6V to 0.9V.

[0042] FIG. 36 is a chart depicting power versus voltage with a supply voltage from 0.6V to 0.9V.

[0043] FIG. 37 is a chart comparing efficiency of the disclosed technology.

[0044] FIG. 38 is another chart comparing efficiency of the disclosed technology.

[0045] FIG. 39 is a chart comparing power of the disclosed technology.

[0046] FIG. 40 illustrates a die micrograph of the chip, according to certain aspects of the present disclosure.

[0047] FIG. 41 is a table of specifications of the chip, according to certain aspects of the present disclosure.

[0048] In one or more implementations, not all of the depicted components in each figure may be required, and one or more implementations may include additional components not shown in a figure. Variations in the arrangement and type of the components may be made without departing from the scope of the subject disclosure. Additional components, different components, or fewer components may be utilized within the scope of the subject disclosure.

DETAILED DESCRIPTION

[0049] The detailed description set forth below is intended as a description of various implementations and is not intended to represent the only implementations in which the subject technology may be practiced. As those skilled in the art would realize, the described implementations may be modified in various different ways, all without departing from the scope of the present disclosure. Accordingly, the drawings and description are to be regarded as illustrative in nature and not restrictive.

[0050] Certain aspects of the disclosed technology provides a ray-tracing processor, which supports inverse rendering (IR) for background extraction. Certain key features of the disclosed technology include, but are not limited to: (1) an application-specific integrated circuit (ASIC) rendering processor that embeds end-to-end IR with PBRT solution for AR application on mobile devices, (2) a reconfigurable mixed-precision PE design supporting diverse computing tasks for both IR and RT task, (3) background clustered Field of View (FOV)-focused 3D construction reducing conventional background scene complexity from O(n log n) to O(1), (4) scalable partitioning scheme for complex 3D objects, with an average of 13 \times speed up on test scenes, (5) use of Global RT Scheduler (GRTS) and Global Memory Access Controller (GMAC) to overcome the challenges of irregular memory access pattern and compute resource with overall 684 \times speedup compared with the baseline design. The 28 nm test chip achieves 3.95-28.8 \times higher RT rendering efficiency compared with existing ASIC solutions, enabling real-time PBRT rendering on mobile edge devices.

[0051] FIGS. 1-7 collectively illustrate a computing flow of the disclosed technology. In the first step, as depicted in FIGS. 1-2, a 2D image 10 captured by a regular camera is sent through a CNN-based physical encoder 12 and a CNN-based physical decoder 14 for inverse rendering (IR) to obtain the background physical attributes (PA) maps 16, including four major background physical attribute (PA) maps 18: a surface albedo map 20, a surface normal map 22, a lighting map 24, and a depth map 26. To save the compressed PA map of the background PA maps 18 on chip 28, a background clustering scheme 30 is utilized based on the similarity of neighbor pixel values of the background map (e.g., the background PA maps 18) by applying an average filter. The IR result PA maps 31 are stored in a Physical Attributes MEM (PAMEM) 32 of the chip 28. In certain aspects, the chip 28 is an ASIC. Each processing element (PE) 34 accessing the PAMEM 32 passes through the Per Pixel Compression Decoder (PPCD) 36 and the Unified Address Converter (UAC) 38 to fetch the corresponding background physical attributes 16 parameter based on the PE task ID 40 from the global ray-tracing scheduler (GRTS) scheme. One PE 34 is one of the many processing cores of the chip 28. In this way, 145-4800 \times of memory saving for different backgrounds is achieved with 0.06% hardware overhead compared with the baseline design. In the second step, as depicted in FIG. 3, the IR result PA maps 31 are used for Camera FOV-focused 3D construction 42.

[0052] With reference to FIGS. 4-7, the constructed 3D background scene 44 is constructed only for the 3D space covered by the user camera FOV 46. In this way, the constructed 3D background scene 44 complexity is reduced from O(n log n) to O(1) compared with conventional RT solutions. In the last step, Physically Based Ray-Tracing

(PBRT) rendering **48** is implemented to render 3D virtual objects with 76% RT workload reduction compared with conventional RT solutions. With reference to FIG. 5, a PBRT flow diagram **50** of the PBRT rendering **48** process is depicted including a ray generation step **52**, an intersect computation step **54** (e.g., bounding box intersection and triangle intersection), a light transportation effect step **56** (e.g., reflection and refraction), and a shading for object step **58** (e.g., diffuse lighting, specular lighting, ambient lighting, and shadow). FIG. 6 schematically illustrates details of the ray generation step **52** of FIG. 5. FIG. 7 illustrates an example ray-tracing computing flow diagram **60**, which begins with the ray generation step **52** for each PE **34**. After the ray generation step **52**, the process proceeds to step **62** for Bounding Box (BBOX) intersect. From step **62**, the process proceeds to step **64** for Object intersect. If a miss is determined, as depicted at box **66**, the process proceeds from step **64** to step **68** for scene intersect and then to step **70** for iterative traversal. On the other hand, if a closet hit is determined, as depicted at box **72**, the process proceeds from step **64** to step **70** for iterative traversal. From step **70**, the process proceeds to step **74** for shading and then to step **76** for result.

[0053] FIG. 8 schematically illustrates comparison charts **78** for comparing conventional RT workload versus RT workload of the present disclosure.

[0054] FIG. 9 illustrates a background scene memory requirement chart **80**.

[0055] FIG. 10 illustrates the top-level architecture of the disclosed technology. To increase the utilization of the PE **34** and address the irregular access background scene memory requirement chart pattern to memory, an 8x6 PE array **82**, for example, is implemented with a global ray-tracing scheduler (GRTS) **84** and a global mem access controller (GMAC) **86**. To support computation for both RT mode **88** and IR mode **90**, a reconfigurable mixed-precision PE **92** is utilized, as illustrated in FIG. 11 and FIG. 12, respectively. Each reconfigurable mixed-precision PE **92** includes a local PE Controller **94**, a clock-gating control **96**, a computing core **98**, which supports 8b, 16b, and 32b MAC **102**, a 64b division module **104**, and 64b square root operations module **106**, and a local OBJMEM memory **108**. Clock gating, via the clock-gating control **96**, disables excessive computing units and local MEM in the IR mode **90** and the RT mode **88** with 32% power saving.

[0056] FIG. 13 illustrates the local PE Controller **94** of each reconfigurable mixed-precision PE **92**, which includes a ray-tracing intersection hashmap decoder (RIHD) **110** and a ray-tracing controller (RTC) **112**.

[0057] FIG. 14 is a first diagram **114** illustrating PA map memory saving with background clustering by mem size.

[0058] FIG. 15 is a second diagram **116** illustrating background clustering scheme HW overhead by area.

[0059] A scalable 3D model partitioning flow **118**, in the RT mode **88**, will be described with reference to FIGS. **16-19** including the schematic diagram **120** of FIG. **16**. In contrast to the conventional solution that builds the BBOX acceleration structure with $O(n \log n)$ complexity, the disclosed technology provides two types of object Bounding Box (BBOX): Empty BBOX (EBBOX) **122** and Target BBOX (Tbbox) **124**. The EBBOX **122** is only used for light transportation estimation and shadow purposes **126**, while the shading computation **128** is skipped. The Tbbox **124** includes a sub-group of user-defined objects inside.

With reference to FIG. **19**, after the BBOX Intersection Evaluator (BBIE) **130** detects intersection with Tbbox **124**, the Triangle Mesh Intersection Evaluator (TIE) **132** computes the ray-triangle intersection **134**, and the result is sent for shading computing. With this scheme, complex 3D objects can be segmented for RT processing without losing the ray-tracing effect. As a result, an $O(1)$ scalability in RT rendering time and an average 13x speed up with only 5.6% memory overhead is achieved compared with the baseline design. FIG. **18** is a speed up with model partitioning chart **136** illustrating normalized run time in percentage versus intersection evaluation, shading, and cast ray for test objects. [0060] FIG. **20** is an on-chip memory overhead for BBOX chart **138** illustrating model size versus memory overhead. [0061] FIG. **21** is 3D model with scalability runtime chart **140** illustrating runtime in seconds versus model size. [0062] FIG. **22** is 3D model without scalability runtime chart **142** illustrating runtime in seconds versus model size. [0063] FIG. **23** depicts on-chip data movement on the chip **28** in the IR mode **90**. FIG. **24** depicts on-chip data movement on the chip **28** in the RT mode **88**. In IR inference mode **144** of the IR mode **90**, double input data **146** and double weight stationary data **148** are supported. In RT mode status mode **150** of the RT mode **88**, as depicted in FIG. **25**, multiple PEs have memory access conflicts. To address the global PAMEM **32** access conflict and increase PE utilization, the GRTS **84** and the GMAC **86** are implemented. With the RT Token Checker (RTTC) **152** checking one PE status every clock cycle, as depicted in FIG. **26**, the GRTS **84** and the GMAC **86** process the RTTC selected PE request individually while the GRTS **84** refreshes the checked PE status if the computation is done. In this way, it achieves 42.8x overall speed up from the GRTS **84**, as depicted in the chart **154** in FIGS. **27**, and 16x overall speed up from the GMAC **86** compared with the baseline design by introducing only 2.8% and 0.6% hardware cost, as depicted in the chart **156** in FIG. **28**.

[0064] The detailed RT shading algorithm **158** to compute the color of each pixel will be described with reference to FIGS. **29** and **30**. RT shading demands complex operations, such as sqrt and division. A PE Compute Unit (PCU) **160** is implemented inside each PE **34**. As shown in FIG. **30**, data from the PAMEM **32** and data from the OBJMEM **108** are sent to the PCU **160** for shading computation. The PCU output **162** from the PCU **160** is stored in a local shading register **164** for lighting effect accumulation. By implementing the PCU **160** in each PE **34**, all the RT computation can be finished individually inside each PE **34**.

[0065] A 28 nm test chip (e.g., the chip **28**) is provided with 0.9V nominal supply voltage. FIG. **31** is a schematic diagram **168** illustrating the total runtime breakdown for the IR-RT flow and demonstrates the background clustering scheme **30** by showing the background reflection is able to light up the object properly by using clustered PA map compared with the baseline design with the detailed background PA map. FIG. **32** is an inverse render INF average quantization accuracy loss chart **169** depicting relative accuracy for the lighting map **24**, the surface albedo map **20**, the surface normal map **22**, and the depth map **26**. With reference to FIG. **33**, four virtual object insertion examples with a teacup **170**, an Utah teapot **172**, a Stanford bunny **174**, and four spheres **176** are demonstrated using the IR-RT rendering scheme. Different materials, such as glass, mirror and ivory are displayed with photorealistic rendering effects of

reflection, refraction and shadow. The IR-RT flow achieves an average of 26 fps for real-time RT rendering with complex 3D objects. A RT AR object insertion case without IR inference is also shown in FIG. 5. Four spheres with different materials are inserted. With reference to the schematic diagram 178 of FIG. 34, photorealistic effects of refraction, reflection and object shadow are properly rendered to the image with 78 FPS, meeting the requirement of real-time AR applications.

[0066] FIGS. 35-39 show measurement and comparison results. FIG. 35 is a frequency versus voltage chart 180 with a supply voltage from 0.6V to 0.9V. FIG. 36 is a power versus voltage chart 182 with a supply voltage from 0.6V to 0.9V. 500 fps/W and 1418 fps/W power efficiency is achieved at 0.9V for the IR mode 90 and the RT mode 88, respectively. FIG. 37 is a comparison chart 184 comparing efficiency of the disclosed technology. FIG. 38 is another comparison chart 186 comparing efficiency of the disclosed technology. FIG. 39 is yet another comparison chart 188 comparing power of the disclosed technology. The disclosed technology implements IR-RT-based rendering solutions, achieving 28.8 \times and 3.95 \times higher ray-tracing PBRT on mobile edge devices.

[0067] FIG. 40 is a die micrograph 190 of the chip 28. FIG. 41 is a table 192 depicting specifications of the chip 28.

[0068] To illustrate the interchangeability of hardware and software, items such as the various illustrative blocks, modules, components, methods, operations, instructions, and algorithms have been described generally in terms of their functionality. Whether such functionality is implemented as hardware, software or a combination of hardware and software depends upon the particular application and design constraints imposed on the overall system. Skilled artisans may implement the described functionality in varying ways for each particular application.

[0069] As used herein, the phrase “at least one of” preceding a series of items, with the terms “and” or “or” to separate any of the items, modifies the list as a whole, rather than each member of the list (e.g., each item). The phrase “at least one of” does not require selection of at least one item; rather, the phrase allows a meaning that includes at least one of any one of the items, and/or at least one of any combination of the items, and/or at least one of each of the items. By way of example, the phrases “at least one of A, B, and C” or “at least one of A, B, or C” each refer to only A, only B, or only C; any combination of A, B, and C; and/or at least one of each of A, B, and C.

What is claimed:

1. An application-specific integrated circuit (ASIC), comprising:
 - a processing element (PE) array;
 - a global ray-tracing scheduler (GRTS) in communication with the PE array;
 - a global memory access controller (GMAC) in communication with the PE array and the GRTS;
 - a physical attributes MEM (PAMEM) in communication with the GRTS; and
 - a reconfigurable mixed-precision processing element of the PE array configured to support an inverse rendering mode for background extraction and a ray-tracing mode.

2. The ASIC of claim 1, wherein, in the inverse rendering mode, the PE array is configured to perform physically based ray-tracing (PBRT) rendering for an augmented reality (AR) application.

3. The ASIC of claim 2, wherein the PBRT rendering comprises ray generation, intersect computation, light transportation effect, and shading.

4. The ASIC of claim 1, wherein the reconfigurable mixed-precision element of the PE array comprises a local processing element controller, a clock-gating control, a computing core, and a local OBJMEM memory.

5. The ASIC of claim 4, wherein the clock-gating control is configured to disable excessive computing units and local MEM.

6. The ASIC of claim 4, wherein each PE of the PE array comprises a PE compute unit configured for shading computation.

7. The ASIC of claim 6, wherein the PE compute unit is configured to receive data from both the PAMEM and the local OBJMEM memory.

8. The ASIC of claim 4, wherein the computing core supports a division module.

9. The ASIC of claim 4, wherein the computing core supports a square root operations module.

10. The ASIC of claim 1, wherein, in the ray-tracing mode, the reconfigurable mixed-precision element of the PE array is configured to perform a scalable 3D model partitioning flow.

11. A mobile device, comprising:
application-specific integrated circuit (ASIC) comprising,
a processing element (PE) array;
a global ray-tracing scheduler (GRTS) in communication with the PE array;
a global memory access controller (GMAC) in communication with the PE array and the GRTS;
a physical attributes MEM (PAMEM) in communication with the GRTS; and
a reconfigurable mixed-precision processing element of the PE array configured to support an inverse rendering mode for background extraction and a ray-tracing mode.

12. The mobile device of claim 11, wherein, in the inverse rendering mode, the PE array is configured to perform physically based ray-tracing (PBRT) rendering for an augmented reality (AR) application.

13. The mobile device of claim 12, wherein the PBRT rendering comprises ray generation, intersect computation, light transportation effect, and shading.

14. The mobile device of claim 11, wherein the reconfigurable mixed-precision element of the PE array comprises a local processing element controller, a clock-gating control, a computing core, and a local OBJMEM memory.

15. The mobile device of claim 14, wherein the clock-gating control is configured to disable excessive computing units and local MEM.

16. The mobile device of claim 14, wherein each PE of the PE array comprises a PE compute unit configured for shading computation.

17. The mobile device of claim 16, wherein the PE compute unit is configured to receive data from both the PAMEM and the local OBJMEM memory.

18. The mobile device of claim 14, wherein the computing core supports a division module.

19. The mobile device of claim **14**, wherein the computing core supports a square root operations module.

20. The mobile device of claim **11**, wherein, in the ray-tracing mode, the reconfigurable mixed-precision element of the PE array is configured to perform a scalable 3D model partitioning flow.

* * * * *